The Doctoral Thesis

Control of spatio-temporal patterns in a spherical field

球形の自律振動子における時空間パターンの制御

Masakazu Kuze

久世 雅和

Graduate School of Integrated Sciences for Life, Hiroshima University

広島大学大学院 統合生命科学研究科

Table of Contents

Publication List

1. 公表論文

(1) M. Kuze, Y. Hiranishi, Y. Okamoto, A. Shioi, and S. Nakata, “Coupling of Two Microbeads Exhibiting Different Features of Oscillations in the Belousov-Zhabotinsky Reaction”, *Chemistry Letters* **2019**, *48*, 847–850.

(2) M. Kuze, M. Horisaka, N. J. Suematsu, T. Amemiya, O. Steinbock, and S. Nakata, “Switching between Two Oscillatory States Depending on the Electrical Potential”, *The Journal of Physical Chemistry B* **2021**, *125*, 3638−3643.

(3) M. Kuze, H. Kitahata, and S. Nakata, “Traveling Waves Propagating through Coupled Microbeads in the Belousov-Zhabotinsky Reaction”, *Physical Chemistry Chemical Physics* **2021**, *23*, 24175−24179.

2. 参考論文

(1) M. Kuze, H. Kitahata, O. Steinbock, and S. Nakata, “Distinguishing the Dynamic Fingerprints of Two- and Three-Dimensional Chemical Waves in Microbeads”, *The Journal of Physical Chemistry A* **2018**, *122*, 1967−1971.

(2) M. Kuze, M. Horisaka, N. J. Suematsu, T. Amemiya, O. Steinbock, and S. Nakata, “Chemical Wave Propagation in the Belousov-Zhabotinsky Reaction Controlled by Electrical Potential”, *The Journal of Physical Chemistry A* **2019**, *123*, 4853−4857.

Chapter 1: General Introduction

1-1. Backgrounds

The non-equilibrium system can exhibit a lot of spatio-temporal dynamics, for example, propagating reaction-diffusion waves in single cells[1] or in cell aggregation.[2] The propagating waves not only contribute the signal transduction over large distances but also perform other functions, for example, the positioning of the division-plane during cell division in a living system. Living organisms can also organize spatio-temporal structures, i.e., rhythms and patterns which are the periodical phenomena on time and space, respectively. Famous examples are circadian rhythms or animal skin patterns.[3-5] Wave propagating phenomena are well known, for example, the calcium waves form the spiral patterns in *Xenopus laevis* oocytes.[6] Wave propagation is also utilized in the somite formation, which are repetitive structures including vertebrae and ribs. Somite is periodically generated from the unsegmented presomitic mesoderm (PSM). PSM cells are coupled to each other to initiate oscillation waves that induce the formation of segmentation boundaries.[7-9]

In addition, these waves can propagate across several cells, and this allows us to observe a “synchronization”. This phenomenon is that the oscillation periods change the same and the phase difference becomes constant when two or more oscillators are coupled.[10,11] Synchronization is also observed in contractile cardiac muscle cells.[12] The pacemaker cell is connected to neighboring contractile cells, and it can regulate the rhythm of the heart contractions. A network of cardiomyocytes enables the rapid transmission of electrical impulses in a coordinated contraction. However, synchronized rhythm collapses when cardiac arrhythmias or fibrillation occurs, and controlling such

complex spatio-temporal dynamics is extremely difficult due to the nonlinear interaction.[13-16]

As shown above, living organisms utilize the oscillations well to create the inhomogeneous distribution of concentrations. However, it is difficult for us to reproduce or control them in chemical experimental systems since the phenomena which exist in nature are so complicated. To dissolve this problem, the unique chemical reaction was investigated for the last several decades. The Belousov-Zhabotinsky (BZ) reaction is the oscillatory chemical reaction, and exhibits not only temporal oscillations but also spatial patterns spontaneously.[17-19] Concentrations of important compounds, i.e., the activator ($HBrO_2$) and the inhibitor (Br^-), increase and decrease alternately and periodically far from the thermodynamic equilibrium. The redox states of the catalyst can visualize self-organized pattern formation and wave excitation such as target patterns, rotating spiral waves,[20] and scroll waves which are continuous stacks of spirals in three dimensions.[21]

After the BZ reaction was found by B. P. Belousov in 1958, pattern formation was observed not only in spatially extended solutions but also droplets[22–24] or gels.[25,26] The BZ droplets organize the cell-like units, and can exhibit the self-propelled motions, changes of their shapes, and even chemotaxis.[23,24.27–30] These features have great potential for the establishment of nonbiological systems such as active cargo transport. The redox states of the catalyst determine the droplets' motion, and thus, it can be reflected in the internal wave pattern.[28-30]

Also, chemical waves can be confined to cation-exchange resin beads[31–33] and sheet,[34] which are referred to as Dowex and Nafion, respectively. They can be loaded with a metal catalyst for BZ reaction, such as ferroin ($Fe[(phen)_3]^{2+}$), and it enables to observe spatial patterns easily. Especially, the former system, the BZ bead system, was studied

widely after Maselko and Showalter firstly reported in 1989.[31] They observed rotating spiral waves on the surface of the ferroin-doped bead when the BZ bead was soaked into the BZ solution without the catalyst. Aihara and Yoshikawa reported that either spatially homogeneous or inhomogeneous pattern was observed in the BZ beads, and their appearance depends on the size of the bead.[33] Uniform excitation over the entire bead was referred to as global oscillations (GO), and occurred in small beads whose diameter was smaller than 0.62 mm. By contrast, chemical waves, including spirals, were initiated from the one edge of the BZ bead and propagated across the bead when the diameter of the bead was larger than 0.8 mm. Also, the mathematical models for the propagation and meandering of waves on a sphere were proposed.[35,36]

In addition, the BZ bead system has been utilized to investigate the synchronization of several oscillators.[37-39] In this experiment, the spatial arrangements of the beads in the BZ solution, especially the distance between the beads, are the key factor for the emergence of their synchronized patterns.[37–41] Researches for the understanding of the wave dynamics in small media can awake interest for engineering applications, such as artificial intelligence (AI) or chemical networks.[42-45] In particular, the latter is also known as a chemical computer or a chemical brain,[46] since that is similar to the neural networks.

1-2. The Purpose of This Thesis

Based on these technological and biological motivations, the aim of this thesis is to investigate the spatio-temporal pattern formation on/in the spherical beads loaded with the catalyst for the BZ reaction. In addition, this study reveals that the self-organized patterns on/in the BZ beads can be controlled by distribution of chemicals produced with

the BZ reaction. In this thesis, the following three studies were carried out.

In chapter 2, the improved BZ bead system is proposed to observe the wave propagation in the small spherical bead. Here, ferroin is selectively loaded into the surface or the entire volume of the bead, as a result, the distribution of them can be controlled.

Chapter 3 represents the self-organization of the patterns in the coupled BZ beads. The coupling of beads can control the distribution of chemical species, and this allows us to observe the spontaneous generation of the chemical waves. This study shows that changes in the direction of the waves can be discussed based on the reaction-diffusion dynamics.

Finally, the electrochemical control in the BZ bead system is introduced in chapter 4. I apply the electrical potential to the bead to switch the oscillatory patterns in the BZ bead, i.e., from GO to TW, and vice versa. I would like to discuss the change in the generation point of the chemical wave in relation to the electrochemical reaction or interaction.

Chapter 2: Distinguishing the Chemical Wave Propagation in Two- and Three-Dimensional Spherical Fields

2-1. Introduction

In the BZ bead system, several spatio-temporal patterns, i.e., global oscillations (GO) and traveling wave (TW), were reported in the previous studies. These wave phenomena can be observed either in the vicinity of the surface or in the entire volume of the BZ bead. However, the differences between the pseudo-two (2D) and three-dimensional (3D) wave propagation are not clarified yet, although these dynamics are interesting and important issues.

Nonlinear chemical systems with spatially controlled catalyst distributions enable us to clarify not only their interesting dynamics but also spatio-temporal structures on wave propagation. In this study, I prepared the two types of the BZ beads which were loaded with ferroin either into the surface or the volume of the beads, and it allows to observe the various spatio-temporal oscillations both in 2D and 3D systems.

2-2. Experiments

Materials

Malonic acid (MA), 1,10-phenanthroline (phen), and iron(II) sulfate heptahydrate ($FeSO_4 \cdot 7H_2O$) were purchased from Wako Pure Chemical Industries, Japan. 10.25 M Sulfuric acid (H_2SO_4) and sodium bromate ($NaBrO_3$) were obtained from Nacalai Tesque, Japan. These reagents were used without further purification. Cation-exchange resin beads (Dowex 50W-X4, U.S.A., average diameter: 0.86 mm) were obtained from Sigma-Aldrich, USA.

In order for the preparation of $Fe(phen)_3^{2+}$ (ferroin) solution, $FeSO_4$(II)$\cdot 7H_2O$ and phen were mixed by 1:3 molar ratio.

Preparation for the "BZ bead"

Cation-exchange resin beads (1 g) were immersed into a 1.1×10^{-3} M aqueous ferroin solution (10 mL) for 1 hour under gentle stirring to load with ferroin into the bead. This procedure was carried out at room temperature. After this process, the solution became colorless, as a result, 4.9×10^{-9} mol of ferroin was loaded to each individual bead. Figure 2-1a shows a schematic illustration of preparation for the BZ bead. Figure 2-1b shows the snapshots of the cross-section of the bead for different loading times. To obtain these images, the ferroin-loaded beads were sliced using two razor blades. Two blades were separated by a spacer (size of the spacer: around 0.1 mm). One hour after the loading, ferroin was localized on and near the surface of the bead (see Figure 2-1b-1). I refer to this situation as a "2D-loaded bead". The 2D-loaded beads were used for the examination immediately after preparation to observe spatiotemporal oscillations on the surface of the bead. Alternatively, I preserved the 2D-loaded bead in distilled water for more than 48

hours. During this process, ferroin was loaded throughout the bead volume homogeneously (see Figure 2-1b-3). This second situation will be referred to as a "3D-loaded bead". The 3D-loaded bead was used to observe spatiotemporal oscillations within the whole body of the bead. Figure 2-1c shows the distributions of ferroin across the sliced bead for different loading times. According to these data, I can estimate the diffusion coefficient of ferroin in the cation-exchange region as ~ 3.5×10^{-8} mm^2 s^{-1} by fitting.

Observation and analysis of the oscillations

The BZ bead was soaked into a catalyst-free BZ solution to observe the oscillations for the BZ beads. The BZ solution consisted of 0.4 M MA, 0.2 M $NaBrO_3$, and 1.0 M H_2SO_4 (depth of BZ solution: 5 mm). 2 hours were required to obtain stable oscillations after the BZ beads were soaked into the BZ solution. The spatio-temporal oscillations on/in the BZ beads were monitored with two digital video cameras (SONY, HDR-CX590V and HDR-CX485, Japan) from top and side simultaneously. All experiments were carried out at 298 ± 1 K. A light source (Trytec, Treviewer B4-400, Japan, the light intensity: 580 lx) was used to enhance the color or the contrast in the oscillations on/in the BZ bead. The light intensity was negligibly low, although the ferroin-catalyzed BZ reaction was photo-sensitive.[47]

Oscillatory phenomena could be visualized by color change due to the reduction and oxidation of ferroin in the BZ reaction. They were analyzed spatiotemporally using ImageJ software (National Institutes of Health, USA.). The following analyzing steps were used to enhance spatio-temporal patterns within or on the bead: (i) the brightness of every image was evaluated as the brightness of the green color channel and (ii) difference images were computed from video frames taken at a time interval of 2/3 s.

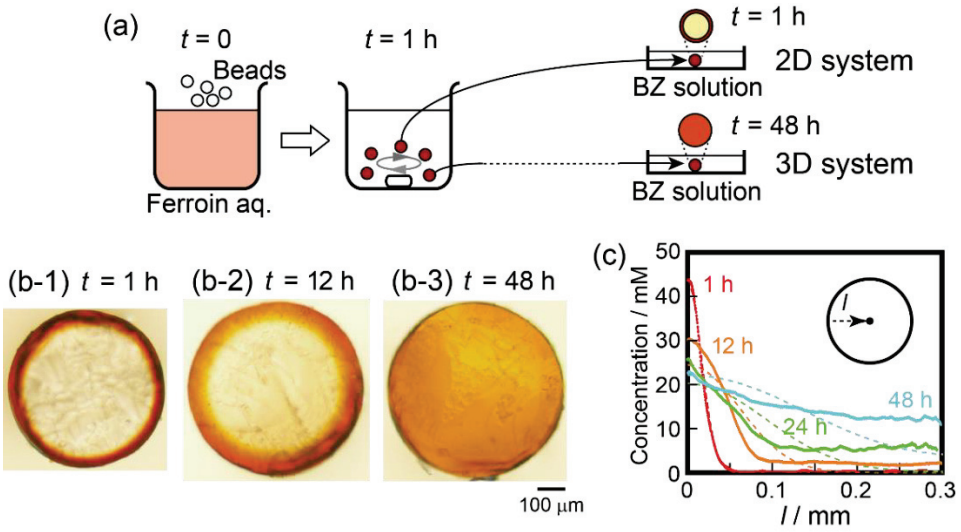

Figure 2-1. (a) Schematic illustration of the preparation of two types of BZ bead systems. (b) Images of sliced BZ beads (thickness: ~ 0.1 mm) at t = (1) 1 h, (2) 12 h, and (3) 48 h after starting loading with ferroin to the cation-exchange resin bead. (c) Concentration of ferroin depending on l (distance from the surface of the bead toward the center of the bead) for different t. Solid curves were obtained from the images in (b). Dotted curves were obtained by theoretical estimation considering diffusion inside a bead.

2-3. Results and Discussion

2-3-1. Classification of patterns

I examined the observation of the spatio-temporal patterns for single 2D- and single 3D-loaded beads in the catalyst-free BZ solution to investigate the wave dynamics. The spatio-temporal patterns for the BZ beads were classified into three types, i.e., global oscillations (GO), traveling waves (TW), or spiral/scroll waves (SW). These patterns appeared in the 2D- or 3D-loaded bead whose diameter was 0.4−1.2 mm. I observed the spontaneous occurrence of GO in both single 2D- and 3D-loaded beads. However, TW appeared in a 3D-loaded bead spontaneously but not in a 2D-loaded system. In order to observe TW in a single 2D-loaded bead, another 2D-loaded bead was put near the 2D-loaded bead. By contrast, I observed the spontaneous appearance of SW in a 2D-loaded bead but not in a 3D-loaded bead. SW in the single 3D-loaded bead were observed only when the 3D-loaded bead was stimulated by an iron needle. The oscillation period of the 2D- and 3D-loaded beads depends on the diameter of the bead.

2-3-2. Global oscillations in single 2D- and 3D-loaded beads

Figure 2-2 shows (a) snapshots and (b) space-time plots of (i) 2D- and (ii) 3D-loaded beads when GO were observed. The space-time plots were generated along a straight line across the center of the bead. Global oscillations appeared spontaneously for both 2D- and 3D-loaded beads under this experimental condition. Spatial phase differences were not observed for the oscillations in the 2D-loaded bead. By contrast, I observed rapid phase waves spreading periodically from the inside outward in the 3D-loaded bead.

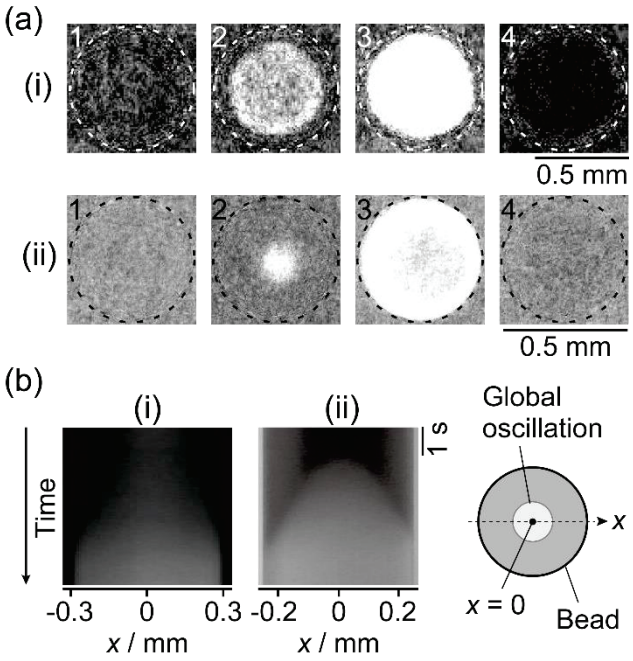

Figure 2-2. (a) Snapshots of (i) 2D- and (ii) 3D-loaded beads when GO was observed (Time interval: (i) 3 s, (ii) 4 s). Dotted lines correspond to the edge of the bead (Diameter of the bead: (i) 0.66 mm, (ii) 0.50 mm). (b) Spatio-temporal plots of the chemical waves in (i) 2D- and (ii) 3D-loaded beads. The spatiotemporal plot was obtained along the *x*-axis, and $x = 0$ corresponds to the center of the bead.

2-3-3. Propagating traveling and spiral waves in single 2D- and 3D-loaded beads

The symmetric distributions of chemical species around the BZ bead were broken by the existence of the neighboring bead. This procedure induced to change the reaction dynamics profoundly, as a result, it allowed us to observe other spatio-temporal patterns besides GO. For example, TW could be observed and was initiated from the point closest to the neighboring bead (left side of the bead), as shown in Figure 2-3a. In addition, SW were also observed when a larger bead whose diameter is more than 0.8 mm was used, as shown in Figure 2-3b. Due to the topological constraints, pairwise tips of spiral

waves were located at approximately the 4 and 10 o'clock positions in the 2D system, as shown in Figure 2-3b-i. By contrast, the single scroll wave propagated across the entire bead volume in the 3D systems, as shown in Figure 2-3b-ii.

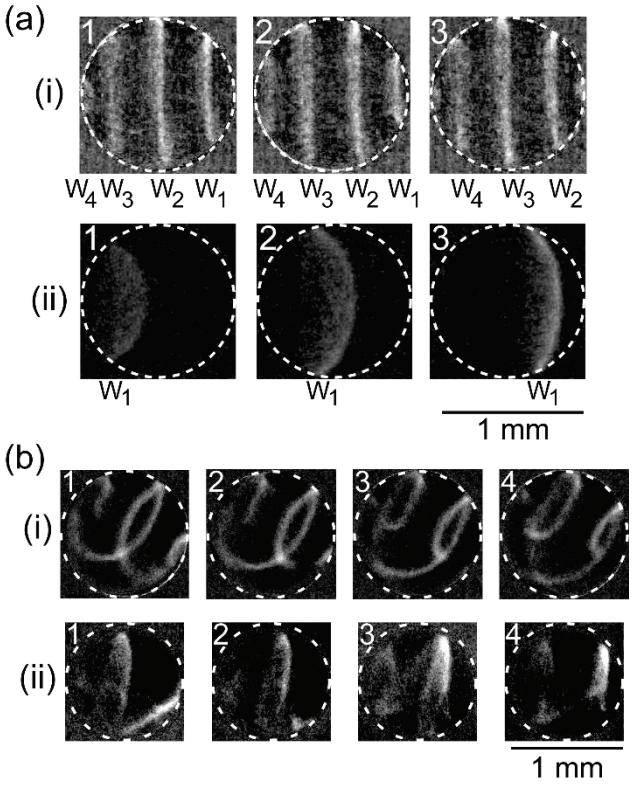

Figure 2-3. (a) Snapshots of (i) 2D- and (ii) 3D-loaded beads when chemical waves propagated (time between frames: 5 s). Diameter of the bead: (i) and (ii) 1.08 mm. W_n (n = 1, 2, 3, or 4) represents the number of the chemical wave. Another loaded bead (not shown) was placed at the left side of the observed bead (the distance between two beads: shorter than 50 μm). (b) Snapshots of (i) 2D- and in (ii) 3D-loaded beads with spiral/scroll waves propagating (time between frames: 3 s). Diameter of the bead: (i) 1.16 mm, (ii) 1.04 mm.

In addition, I investigated the wave velocity along (I) the x-axis or (II) the periphery of (i) 2D- and (ii) 3D-loaded beads, as shown in Figures 2-4-c. The wave velocity along the x-axis became maximum and minimum values at the center ($x = 0$) and at the edge of the bead ($x \sim \pm 0.5$ mm), respectively in the 2D-loaded bead (Figure 2-4I(c-i)). By contrast, the wave velocity along the x-axis was almost constant for every location on the x-axis in the 3D-loaded bead (Figure 2-4I(c-ii)). If the chemical waves propagate on the surface of the bead at a constant velocity ($v_{\{2D\}}$), the velocity along the x-axis, v_x, is given as

$$v_x = \sqrt{1 - \frac{x^2}{R^2}}\ v_{\{2D\}}, \tag{2-1}$$

where R is the radius of the bead. Least-square fitting of eq. 2-1 as shown in the continuous curve in Figure 2-4I(c-i) similarly reproduced the experimental results.

The wave velocity along the periphery in the 2D-loaded bead was almost constant for every location, as shown in Figure 2-4II(c-i). On the other hand, the velocity along the periphery in the 3D-loaded beads drastically increased depending on $|\theta|$, as shown in Figure 2-4II(c-ii). If the chemical waves propagate across the bead volume at a constant velocity, the velocity along the periphery of the bead, v_s, is expressed by

$$v_s = \frac{v_{\{3D\}}}{\cos(\theta/2)}\ , \tag{2-2}$$

where $v_{\{3D\}}$ is the velocity of the waves propagating in the 3D-loaded bead. The fitted curve obtained by eq. 2-2 agreed very well with the experimental results, as shown in Figure 2-4II(c-ii).

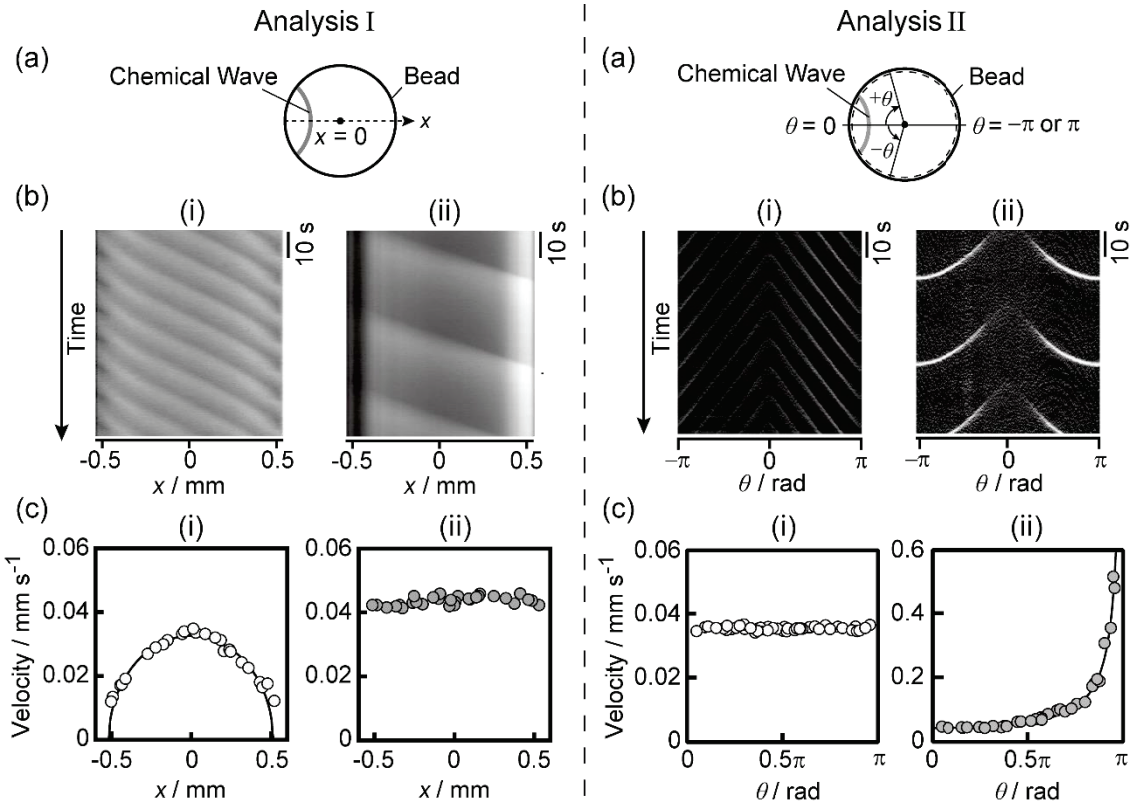

Figure 2-4. (a) Schematics representing the definition of variables. (b) Space−time plots of propagating chemical waves for (i) 2D- and (ii) 3D-loaded beads based on Analyses I (left half) and II (right half). These plots were generated along the *x*-axis (Analysis I) or the periphery of the beads (Analysis II). The data for (i) and (ii) correspond to those for (i) and (ii) in Figure 2-3a, respectively. (c) The velocity of the chemical wave propagating (i) on 2D (empty circles) and (ii) in 3D (filled circles) -loaded beads based on Analyses I and II. The solid curve in (c-i, left half) for the 2D-loaded bead was obtained by fitting with eq. 2-1 (R = 0.52 mm). I set the fitting parameter, $v_{\{2D\}}$. Here, I obtained $v_{\{2D\}}$ = 0.0330 ± 0.0008 mm s^{-1} from the four trials. The solid line in (c-ii, right half) for the 3D-loaded bead was obtained by fitting with eq. 2-2 (R = 0.52 mm). I set the fitting parameter, $v_{\{3D\}}$. Here, I obtained $v_{\{3D\}}$ = 0.0429 ± 0.0008 mm s^{-1} from the four trials.
Reprinted with permission from *J. Phys. Chem. A* **2018**, *122*, 1967−1971. Copyright 2018 American Chemical Society.

2-3-4. Spatio-temporal oscillations in the 2D- and 3D-loaded beads depending of the diameter of the bead, *d*

Here, the spatio-temporal oscillatory behavior depending on the diameter of the

bead, d, was investigated. Figure 2-5a shows the oscillation period for the 2D-loaded bead as a function of d. The periods of GO became shorter with an increase in d. On the other hand, the periods of SW were almost constant for any d. Figure 2-5b describes the spatio-temporal patterns in the 3D-loaded bead as a function of d. The periods of GO and TW became shorter with an increase in d. Either GO and TW were observed at $d >$ 0.57 mm and $d <$ 0.75 mm, respectively. At the intermediate size range, 0.57 mm $\leq d \leq$ 0.75 mm, the coexistence of GO and TW was observed. This result means that either TW and GO stably appear for at least 2 hours without switching each other.

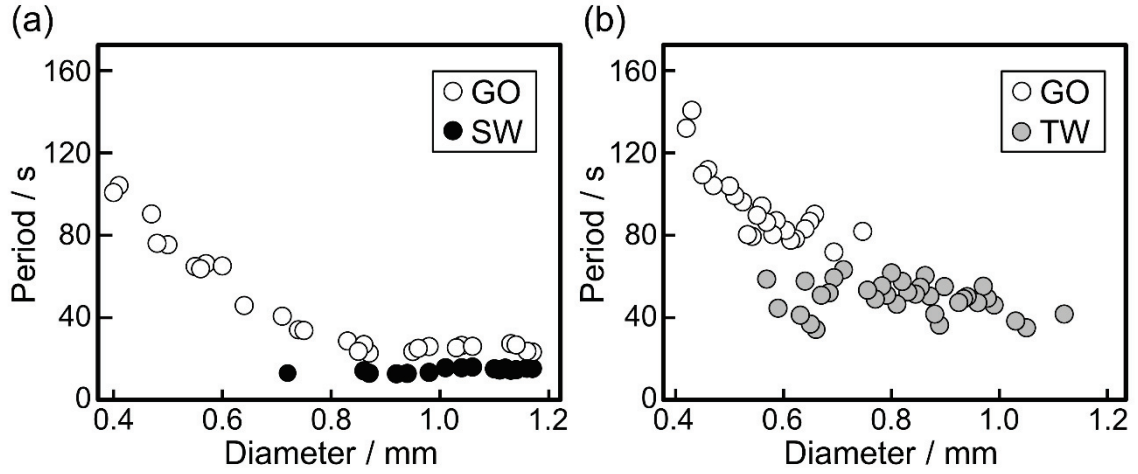

Figure 2-5. Periods of oscillations for (a) 2D- and (b) 3D-loaded beads depending on the diameter of the bead, d. White, gray, and black circles represent GO, TW and SW, respectively.

2-4. Conclusions

In this study, an experimental protocol for the BZ bead system was offered. Either pseudo-two or three-dimensional wave propagation could be observed by the preparation of microbeads loaded with the catalyst for the BZ reaction either on the bead surface or in its entire volume. The results revealed the velocity profiles in the 2D and 3D systems have distinct differences. This study also suggested that the homogeneous oscillations can be broken by the asymmetrical distribution of chemical species or the local external stimulus, and it induced traveling waves or spiral waves.

Chapter 3: Synchronization between Two Coupled Microbeads in the Belousov-Zhabotinsky Reaction

3-1. Introduction

Synchronization can be observed when some oscillators are coupled.[10,11] Not only experimental systems but also theoretical models were developed to clarify the mechanism of synchronization. These studies mainly focused on the temporal change of oscillation, but the spatial information was not enough to be discussed.[48-51]

The BZ bead system is useful for investigation into the interaction between coupled oscillators and discussion on both the spatial and temporal features of wave phenomena in them based on reaction-diffusion dynamics. This system allows for the spatial arrangement of the oscillators. In addition, the diffusion of the catalyst need not be considered. In the previous papers, synchronization was observed as a function of the distance between the BZ beads.[38,39] The distance between the BZ beads is a key factor in the coupled BZ bead system since the changing distance between the beads can control the coupling strengths among the nearest neighboring oscillators.

In this study, we examined the coupling of two BZ beads in the catalyst-free BZ solution to observe characteristic spatio-temporal behavior during synchronization. In addition, we investigated the direction of propagating chemical waves on the BZ beads depending on the minimum distance between two beads, *l*. Here, I selected the BZ beads which exhibited various spatio-temporal patterns, i.e., global oscillations (GO) and traveling waves (TW) in the coupling. In order to elucidate the geometrical effect of

diffusion of the key compound in the BZ reaction by altering *l*, a numerical calculation based on the diffusion dynamics was also performed.

3-2. Experiments

The used reagents were the same as those in chapter 2. I used the 2D- and the 3D-loaded beads to selectively induce GO and TW, respectively. As for the loading concentration, 1 g of the cation-exchange resin bead was soaked into the 10 mL of 1.1 mM ferroin solution. I judged that ferroin was fully loaded into individual beads one hour after the beads were immersed in the ferroin solution since the solution became colorless. The diameter of the beads was 0.6–1.0 mm. In this experimental condition, a single BZ bead on a glass petri dish exhibited TW. The BZ solution consisted of 0.4 M MA, 0.2 M $NaBrO_3$, and 1.0 M H_2SO_4, and was not contained the catalyst. All the experiments were recorded with a digital video camera (SONY, HDR-CX590V, Japan), and monitored with a side view. The obtained data were analyzed with ImageJ software (National Institutes of Health, Bethesda, MD, U.S.A.). The observations were performed at 298 ± 1 K.

In this chapter, the five experiments were carried out.

Experiment 1

At first, I investigated the effect of the plate on which a single BZ bead was placed. Spatio-temporal oscillations of the BZ beads on (a) a glass plate or (b) a silicone rubber plate (thicknesses: (a) 0.1 and (b) 1.0 mm) were monitored.

Experiment 2 (GO-GO coupling)

Next, I coupled the two beads on a silicone rubber plate as a function of the minimum distance between the two beads, l. To alter l, one bead was placed on a silicone rubber plate connected to a stepper motor (COMS, PM80B-100X, Japan, with a minimum precision: 0.2 μm), as shown in Figure 3-1a. The other bead was placed on another silicone rubber plate fixed to the vessel filled with the catalyst-free BZ solution. Here, both the two beads exhibit GO at l was sufficiently long (l > 1 mm).

Experiment 3 and 4 (TW-TW coupling)

In Experiment 3 and 4, I examined the coupling of the two beads which exhibited TW. The difference between them was the propagation directions of TW. The experimental system in Experiment 3 was almost the same as that in Experiment 2, but the two BZ beads on the silicone rubber were in contact with glass plates to induce the generation of TW. The glass plates were placed vertically on silicone rubber plates, as shown in Figure 3-1a. On the other hand, one BZ bead was placed on a PET sheet whose position was controlled by the stepper motor in Experiment 4. The other bead was placed on the other PET sheet which was fixed on the bottom of the rectangular vessel, as shown in Figure 3-1b. Here, only the 3D-loaded beads were used in Experiments 1–4.

Experiment 5 (GO-TW coupling)

In Experiment 5, one 2D- and one 3D-loaded beads were selected to examine the GO-TW coupling. GO and TW were observed in the 2D- and 3D-loaded beads, respectively. The experimental system in Experiment 5 was the same as that in Experiment 4.

In all the experiments of coupling (Experiments 2–5), we altered l stepwise from 1 to 0 mm, and we observed five or more oscillations at each l to calculate the period of oscillations. In addition, we defined the period ratio between the two oscillators as R_p (= P_l / P_s, where P_l is the longer period of one bead and P_s is the shorter period of the other bead.).

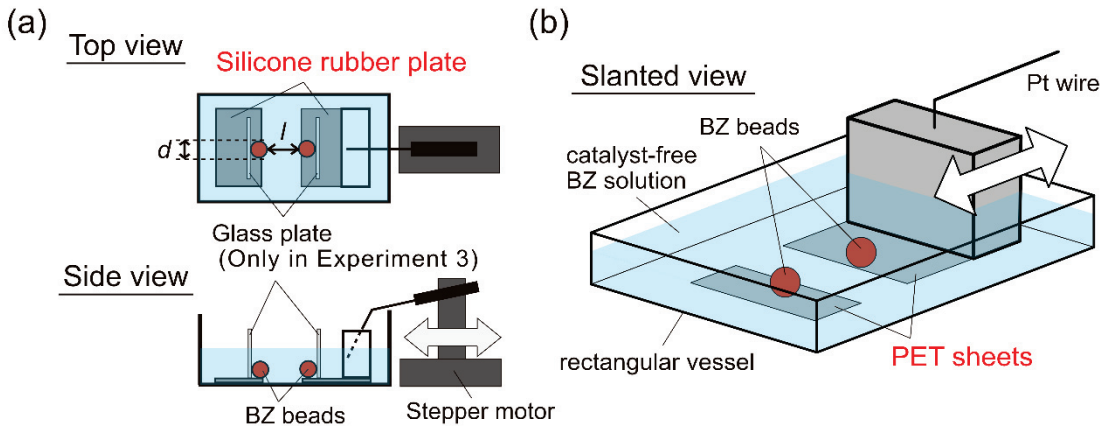

Figure 3-1. Schematic illustration for the experimental setup for (a) Experiments 2 and 3 and (b) Experiments 4 and 5. (a) Two BZ beads were placed on two silicone rubber plates. In order to alter *l*, one silicone rubber plate including one bead was connected to the stepper motor. The other silicone rubber plate was fixed on the bottom of the vessel. In Experiment 3, each glass plate was put vertically on the silicone rubber plate to control the direction of the TW. These glass plates were in contact with the BZ beads. (b) Two BZ beads were placed on two PET plates. A BZ bead was placed on a PET sheet whose position was controlled by the stepper motor. The other bead was fixed on the other PET sheet.

3-3. Results

3-3-1. Oscillations for a single bead placed on a glass or a silicone rubber plate (Experiment 1)

To evaluate the effect of the boundary condition on the BZ oscillations, I observed the spatio-temporal patterns in the BZ bead on the glass and the silicone plate. The range of the diameter of the bead was 0.7–1.0 mm. On the silicone rubber plate, GO mainly appeared and its probability was 82% (the number of experiments, $N = 40$). In the other results (18%), TW were observed and the waves were generated from any edge of the bead. On the other hand, TW appeared on the glass plate in all the experiments ($N = 50$). The TW were initiated from the contact point with the glass plate.

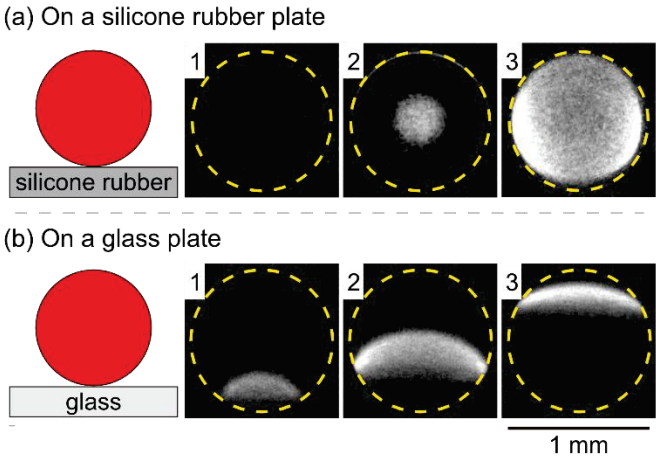

Figure 3-2. Snapshots of spatio-temporal oscillations in the BZ bead on (a) a silicone rubber plate and (b) a glass plate (side view, time interval: 6 s). Diameters of the bead: d = (a) 0.98, and (b) 1.00 mm. Dotted circles correspond to the edges of the beads.

3-3-2. Coupling of two beads which exhibited GO (Experiment 2)

Figure 3-3a shows the snapshots of the coupling of the two beads on the silicone rubber plates. GO was observed for both two beads at $l > 0.12$ mm, but it changed to TW at $l \leq 0.12$ mm. The TW were initiated from the contact point between the two beads and propagated to the opposite sides at $l = 0$ mm, as shown in Figure 3-3a. Figures 3-3c and d represent R_p for the two beads and the periods of the two beads as a function of l, respectively. The oscillation periods became drastically short with a decrease in l at $l \leq 0.12$ mm, as shown in Figure 3-3c. The results that $R_p = 1$ at $l \leq 0.12$ mm, as shown in Figure 3-3d, suggested the bifurcation value of l between synchronization and no synchronization, l_b, was 0.12 mm.

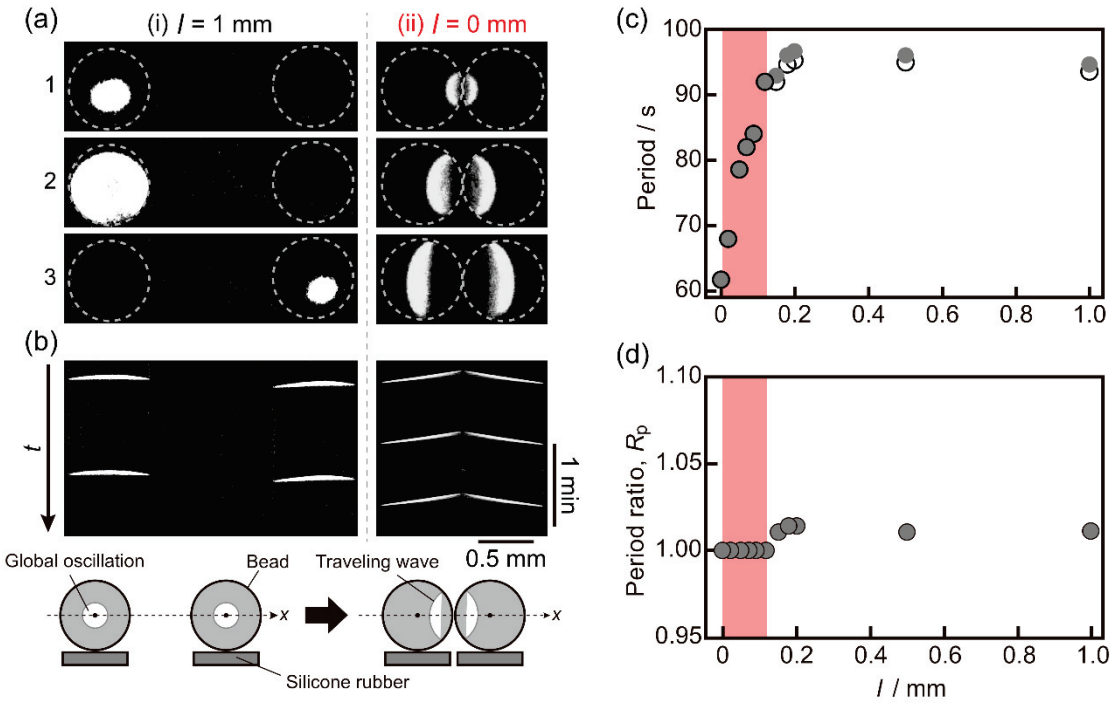

Figure 3-3. Results of coupling of two beads on silicone rubber plates. (a) Snapshots of coupled the two beads with a side view (Diameter of the left and right beads was 0.73 mm.) at l = (i) 1 and (ii) 0 mm (time interval: 3 s). Dotted circles correspond to the edges of the bead. (b) Space-time plots for the chemical waves in the two beads. The space-time

plots were obtained along the x-axis, as shown at the bottom of (b). (c) R_p for the two beads as a function of l. (d) Lower (empty circle) and higher (gray circle) periods of the two beads as a function of l.

2-3-3. Coupling of two beads which exhibited TW (Experiment 3)

In this section, I examined the coupling of the two beads which exhibited TW. Figure 3-4 shows the experimental results of Experiment 3. The TW in both two beads was individually initiated from the contact point with the glass plate when l was long enough, i.e., l = 0.20 mm.

At the initial state of 0.05 mm < $l \leq$ 0.12 mm, indicated by green in Figure 3-4b, the bead with the shorter period exhibited no change, and thus, this bead was regarded as a pacemaker. On the other hand, two traveling waves in the bead with the longer period were generated (see the left bead as shown in Figure 3-4a). One was still initiated from the contact point between the bead and the glass plate. The other appeared from the point closest to the neighboring bead. However, these waves annihilated each other, and the former traveling wave was disappeared. At the steady state, only the traveling waves which initiated from the point closest to the other bead survived, as shown in Figure 3-4a-ii.

Two chemical waves were observed in the bead with the shorter period (the right bead in Figure 3-4a) at the initial state of $l \leq$ 0.05 mm, indicated by blue in Figure 3-4b. One was initiated from the contact point between the bead and the glass plate, and the other from the point closest to the other bead. Eventually, these waves annihilated each other, and the waves initiated only at the point closest to the other bead at the steady state, as shown in Figure 3-4a-iii. That is, the TW in both beads were initiated from the nearest point to the neighboring bead individually.

Figures 3-4c and d represent the periods of two beads and R_p for the two beads, respectively, as a function of l. At 0.05 mm < $l \leq$ 0.12 mm, indicated by green in Fig. 3-4c, the oscillation periods did not change, but periods of both beads became drastically short when l changed shortly at $l \leq$ 0.05 mm. The l_b was considered to be 0.12 mm since R_p was 1 at $l \leq$ 0.12 mm according to Fig. 3-4d. This value was similar to that in Experiment 2.

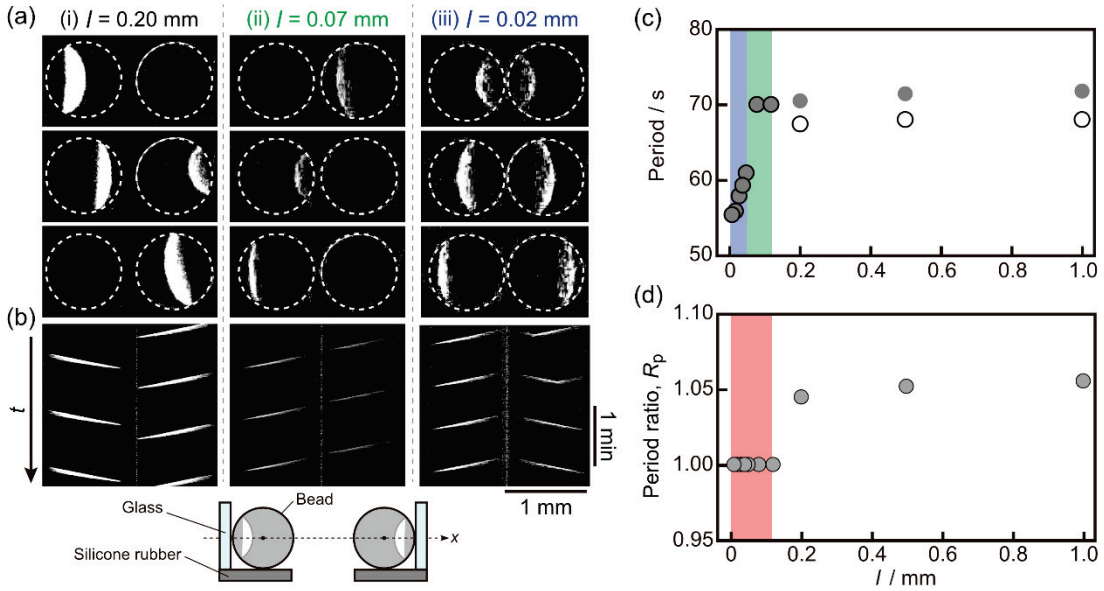

Figure 3-4. Results of coupling of the two beads which is in contact with the glass plates on the silicone rubber plates. (a) Snapshots of two beads (Diameters of the left and right beads were 0.91 mm and 0.92 mm, respectively.) at l = (i) 0.20 mm, (ii) 0.07 mm, and (iii) 0.02 mm (time interval: (i) 5 s, (ii) 9 s, and (iii) 4 s). Dotted circles correspond to the edges of the bead. (b) Spatio-temporal plots on the coupled two beads for different l. They were generated along the x-axis, as indicated schematically. (c) R_p for the two beads as a function of l. (d) Oscillation periods of the two beads as a function of l. Empty and gray circles correspond to shorter and longer periods, respectively.

3-3-4. Coupling of two beads that exhibited TW on the PET sheets (Experiment 4)

In order to induce TW in both beads, I used two equivalent 3D-loaded beads

since TW could be observed in the 3D-loaded bead placed on the PET sheet. The oscillation periods of the selected two beads were different because of individual differences in the beads, so I could not control them experimentally. R_p between the two BZ beads changed for each new experiment, but two equivalent beads were selected, and R_p was controlled lower than 1.25. In the coupled two-bead system, oscillations in one bead with a shorter period can govern the oscillations in the other bead with a longer period. Herein, the former and the latter beads were referred to as the pacemaker and the driven oscillators, respectively.

Figure 3-5 shows the results of the coupling of the two beads whose patterns were TW on the PET sheets. In Figure 3-5a, the period of the right bead was longer than that of the left bead at sufficiently long l ($l > 1$ mm), that is, the left and right beads became the pacemaker and the driven oscillators, respectively. The TW in both beads were initiated from the contact point between the bead and the PET sheet at $l > 0.11$ mm, as shown in Figure 3-5a-3. Figure 3-5b-1 shows the R_p between the two beads as a function of l. I judged that the synchronization was observed when $R_p = 1$. Thus, synchronization was observed at $l \leq 0.11$ mm due to the results in Figure 3-5b-1. The TW in the pacemaker (the left bead in Figures 3-5a-1 and 3-5a-2) were still initiated at the contact point with the PET sheet at $l \leq 0.11$ mm, that is, $\theta = 90°$. Here, θ was the direction of the TW, as indicated by the inset in Fig. 3-5b-2. By contrast, θ for the driven oscillator became around 0° at $l = 0.11$ mm. In addition, θ increased with a decrease in l at $l < 0.11$ mm, as shown in Figure 3-5b-2.

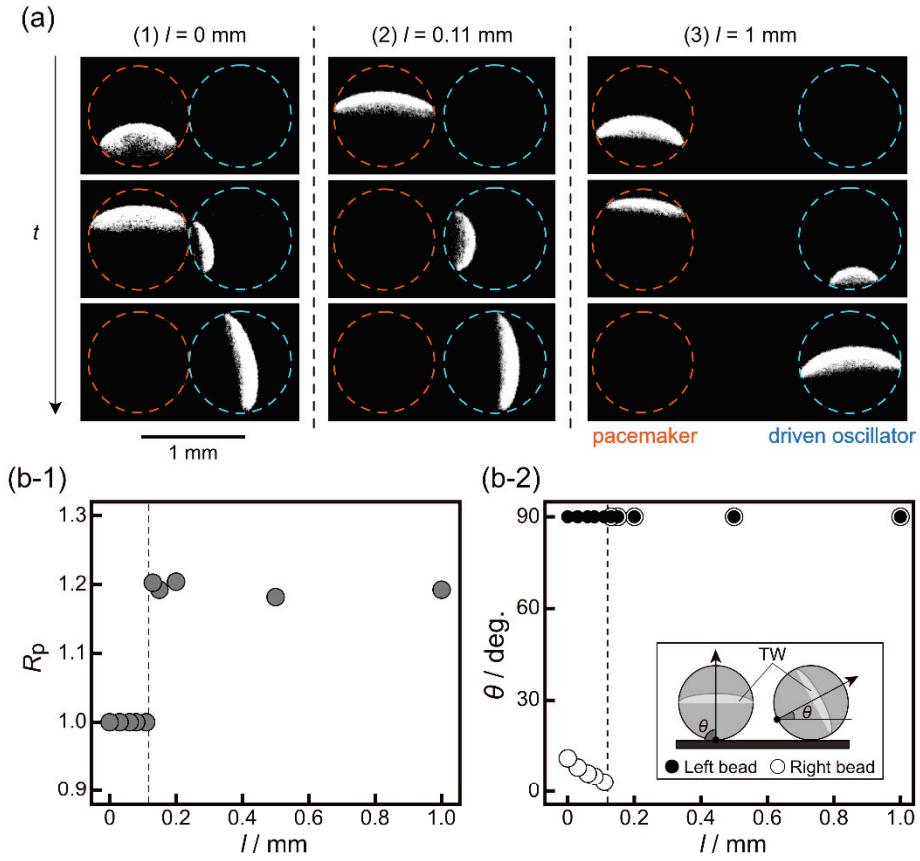

Figure 3-5. Oscillations for two coupled beads which exhibited TW on the PET sheets. (a) Snapshots of the two beads at l = (1) 0, (2) 0.11, and (3) 1 mm (time interval: 8 s). The diameters of the left and right beads were 1.00 and 1.01 mm, respectively. Dashed circles correspond to the edge of the beads. (b) (1) R_p and (2) θ in both the two beads as a function of l. The direction of the TW was represented by the solid arrow in the inset.
Reproduced from *Phys. Chem. Chem. Phys.* **2021**, *23*, 24175−24179. with permission from the PCCP Owner Societies.

3-3-5. Coupling of two beads which exhibited different patterns on the PET sheets (Experiment 5)

One 2D- and one 3D-loaded bead were selected to carry out the coupling between GO and TW. GO were observed in the 2D-loaded bead, but TW appeared spontaneously in the 3D-loaded bead. In the 2D-3D coupling, the 2D-loaded bead became the pacemaker since the period of GO was shorter in comparison to that of TW.

Figure 3-6 shows the oscillatory behavior in the 2D-3D coupling. We could recognize that the two beads oscillated independently at $l > 0.12$ mm. In this case, the contact point between the bead and the PET sheet was the initiation point of the TW in the 3D-loaded bead. On the other hand, the generation point of the TW in the 3D-loaded bead changed at $l \leq 0.12$ mm, as shown in Figures 3-6a-1 and 3-6a-2. The period of TW was different from that of GO at $l > 0.12$ mm, as shown in Figure 3-6b-1. R_p was not 1 at $l > 0.12$ mm, and thus, synchronization did not occur. However, at $l \leq 0.12$ mm, I could observe synchronization since the period of TW became the same as that of GO. The directions of the TW, θ, were 90° under no synchronization, but the TW were initiated from the closest point to the 2D-loaded bead at $l \leq 0.12$ mm, that is, θ changed to 0°.

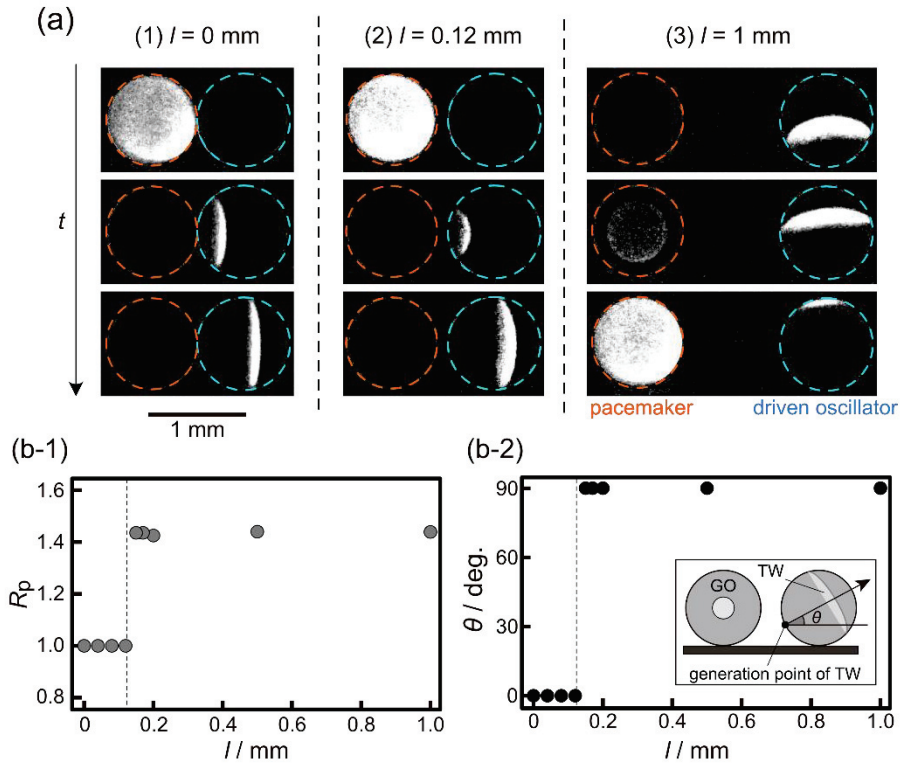

Figure 3-6. Results of the 2D-3D coupling. (a) Snapshots of the two beads (Diameters of the left and right beads were 0.94 and 0.95 mm, respectively.) at l = (1) 0, (2) 0.12, and

(3) 1 mm (time interval: (1) 4, (2) 9, and (3) 8 s). (b) (1) R_p and (2) directions of the TW, θ, propagating on the 3D-loaded bead as a function of l. The solid arrow in the inset represents the direction of the TW.

Reproduced from *Phys. Chem. Chem. Phys.* **2021**, *23*, 24175−24179. with permission from the PCCP Owner Societies.

3-4. Discussion

The results of Experiment 2, as shown in Figure 3-2, shows that GO may be maintained by the silicone rubber plate, and TW were induced by contact with the glass plate. These results suggest that the silicone rubber inhibits or the glass activates the occurrence of the BZ reaction around the contact point between the bead and the plate.

Based on the experimental results and related papers,[37-39] I would like to discuss the interaction between the two BZ beads in the coupled BZ bead system. The oxidation of ferroin in the BZ process autocatalytically produces $HBrO_2$ molecules inside the BZ bead, and $HBrO_2$ molecules subsequently diffuse from the bead to the outer solution. Here, the local concentration of the activator increases around the gap between the two BZ beads when the distance between the two beads is short. The higher concentration of the activator may induce in-phase synchronization. This consideration is agreed with the facts that in-phase synchronization was observed in the similar system and the coupled BZ bead system was classified as excitatory, according to previous researches.[41] The threshold value of l_b (≈ 0.12 mm) is similar to the results reported in the related paper.[38] Here, I should note that the diameter of beads may affect l_b. These data suggest the diffusion of the activator can trigger off ferroin oxidation at the neighboring bead, and its maximum distance is around 0.12 mm.

We can observe the three types of coupled patterns as a function of l in Experiment 3. This result suggests that the occurrence of oxidation at the contact point with the glass plate competes with that at the point closest to the neighboring bead. That is, the concentration of an activator may determine whether the oxidation of ferroin in the BZ reaction at the contact point with the glass plate is prior to that at the point closest to the neighboring bead or not.

Next, we calculated the time difference, Δt (= $|t_L - t_R|$) between the two beads when synchronization was observed. Here, the times t_L and t_R correspond to the time which was required to propagate from a start point of chemical waves to the center of each bead, respectively, as shown in Figure 3-7. The open and filled circles in Figure 3-7 represent the experimental results of Δt in the Experiments 2 and 3, respectively. Δt increased with an increase in l in the Experiment 2. In addition, the experimental results are similar to the following numerical results.

In the Experiment 3, Δt values at $l \leq 0.05$ mm were similar to those in the Experiment 2. However, the Δt at l was around 0.05 mm changed drastically, and Δt values at 0.05 mm $< l \leq 0.12$ mm were several seconds more than those in Experiment 2.

I consider the propagation of the TW in the beads and the activator's diffusion across the gap between the two beads. The time taken for diffusion, t_d, is expressed by eq. 3-1. Here, "time required for diffusion, t_d" is defined as the time taken for the activator to diffuse from the edge of the bead to the edge of the neighboring bead.

$$t_d = \frac{l^2}{D} \qquad (3\text{-}1)$$

where, D (mm^2 s^{-1}) and l (mm) are the diffusion coefficient of an activator (= 2.0×10^{-3} mm^2 s^{-1}) and the diffusion distance.[28] Δt was calculated by using eq. 3-1 and represented by the solid line in Figure 3-7. These values are similar to those in Experiment 2 (see empty circles in Figure 3-7). At 0.05 mm $< l \leq 0.12$ mm in Experiment 3, indicated by green in Fig. 3-7, we should consider the time taken for the TW to propagate in the beads. Therefore, we calculated the time for wave propagation. This corresponds to the sum of t_d and double the time taken for propagation on half of the bead, t_p (see the dotted line and the schematic illustration in Figure 3-7). Here, t_p was calculated using the experimental data in the Experiment 3, which are the values of the velocity of traveling waves (= 0.059

mm s^{-1}). The values of Δt obtained in the Experiment 3 are lower than the numerical results, but are similarly reproduced by the numerical calculation. These results suggest that Δt can be used to distinguish between two types of synchronization.

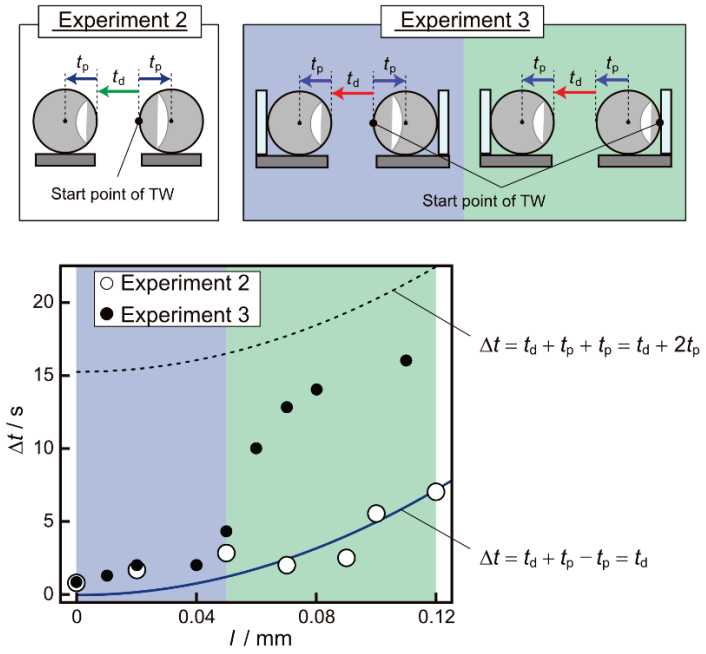

Figure 3-7. The values of Δt in the Experiments 2 and 3 during synchronization. The solid line represents the diffusion time of an activator as a function of l. The dotted line represents the sum of t_d and double t_p as a function of l.

Next, the propagation of the chemical waves over the gap between the two BZ beads is discussed based on the results and related papers.[37-39,41] First, the values of θ are calculated numerically using the following mathematical model.

Numerical calculations on the coupling of the two beads were carried out. Here, the left and right beads were regarded as the pacemaker and the driven oscillator, respectively. Assuming that GO appeared in the pacemaker, the TW were generated at the center of the bead. On the other hand, the TW were generated from the contact point

between the pacemaker and the PET sheet if TW were observed in the pacemaker. The contact point between the PET sheet and the pacemaker corresponded to the origin of the coordinates (point O), as shown in Figure 3-8a. The area where $y < 0$ represented the PET sheet beneath the beads. $(x_l, y_l) = (0, r)$ and $(x_r, y_r) = (2r+l, r)$ correspond to the center positions of the left and right beads, respectively. Here, l and r are the length between the two beads and the radius of the bead, respectively. Based on the dynamics of the diffusion, consumption, and generation of the activator by the reaction, the time evolution equation of the activator concentration $u(x, y, t)$ in a two-dimensional system is described as follows:

$$\frac{\partial u}{\partial t} = D\nabla^2 u - au + b, \tag{3-2}$$

where a and b are the consumption and generation rates of the activator during the BZ reaction, respectively, and D is the diffusion coefficient of the activator. Herein, a is a constant, and D is set to D_{sol}, D_{bead}, and 0 in the solution, beads, and PET sheets, respectively. In addition, I assumed that the activator is produced in the region corresponding to the chemical waves in the pacemaker:

$$b = \begin{cases} b_0 & (vt - W < \sqrt{(x-x_c)^2 + (y-y_c)^2} < vt \\ & \quad \wedge \sqrt{(x-x_l)^2 + (y-y_l)^2} < r) \\ 0 & (\text{otherwise}) \end{cases}, \tag{3-3}$$

where v and W are the speed and width of the chemical waves, respectively. The coordinates (x_c, y_c) describe the initiation points of the TW. Thus, (x_c, y_c) corresponds to the center of the pacemaker if GO appear in the pacemaker, that is, $(x_c, y_c) = (x_l, y_l)$). By

contrast, (x_c, y_c) corresponds to the contact point between the pacemaker and the PET sheet if TW were observed in the pacemaker, that is, (x_c, y_c) = (x_l, 0).

The space and time units were set to 1 mm and 1 s, respectively, in this numerical calculation. The radii of the beads were set to $r = 0.5$ based on the experiments. D in the bulk solution and inside the beads were set to $D_{sol} = 2.0 \times 10^{-3}$ and $D_{bead} = 1.0 \times 10^{-3}$, respectively. Here, I note that literature value of D_{sol} was 2.0×10^{-3} mm s^{-1}.[18] The other parameters were set as $a = 0.2$, $b = 10$, $u_{th} = 0.55$, $v = 0.06$, and $W = 0.05$. Herein, u_{th} is the threshold value of the activator concentration which triggers off the wave initiation in the driven oscillator (the right bead). The Neumann boundary condition was adopted as the region boundary. The mesh size and time step were set to $\Delta x = 0.01$ and $\Delta t = 0.001$, respectively. I assumed that the oscillations in the driven oscillator are observed if the concentration of the activator, u, exceeds u_{th}, and the TW are initiated at the point where u reaches u_{th} earliest among the points on the circumference of the driven oscillator. Here, I should note that I cannot observe the TW in the driven oscillator if u did not exceed u_{th} since the driven oscillator was not oscillatory. Then, the time evolution of the concentration of the activator u was obtained as a function of the points on the circumference of the driven oscillator, φ, at different values of l. The definition of φ was indicated in Figure 3-8a. Here, φ corresponded to θ, which was obtained experimentally, as shown in Figure 3-6.

Figure 3-8b describes the numerical results of the initiation point of the TW. The concentration of the activator, u, at the point on the circumference of the driven oscillator exceeded u_{th} at $l \leq 0.12$ when GO were observed in the pacemaker, as shown in the left side of b in Figure 3-8. In addition, φ, where u initially exceeded u_{th}, was 90° at $l \leq 0.12$. On the other hand, u at the point on the circumference of the driven oscillator exceeded

u_{th} at $l \leq 0.11$ when TW appeared in the pacemaker, as shown in the right side of b in Figure 3-8). In this case, φ increases with a decrease in l at $l \leq 0.11$.

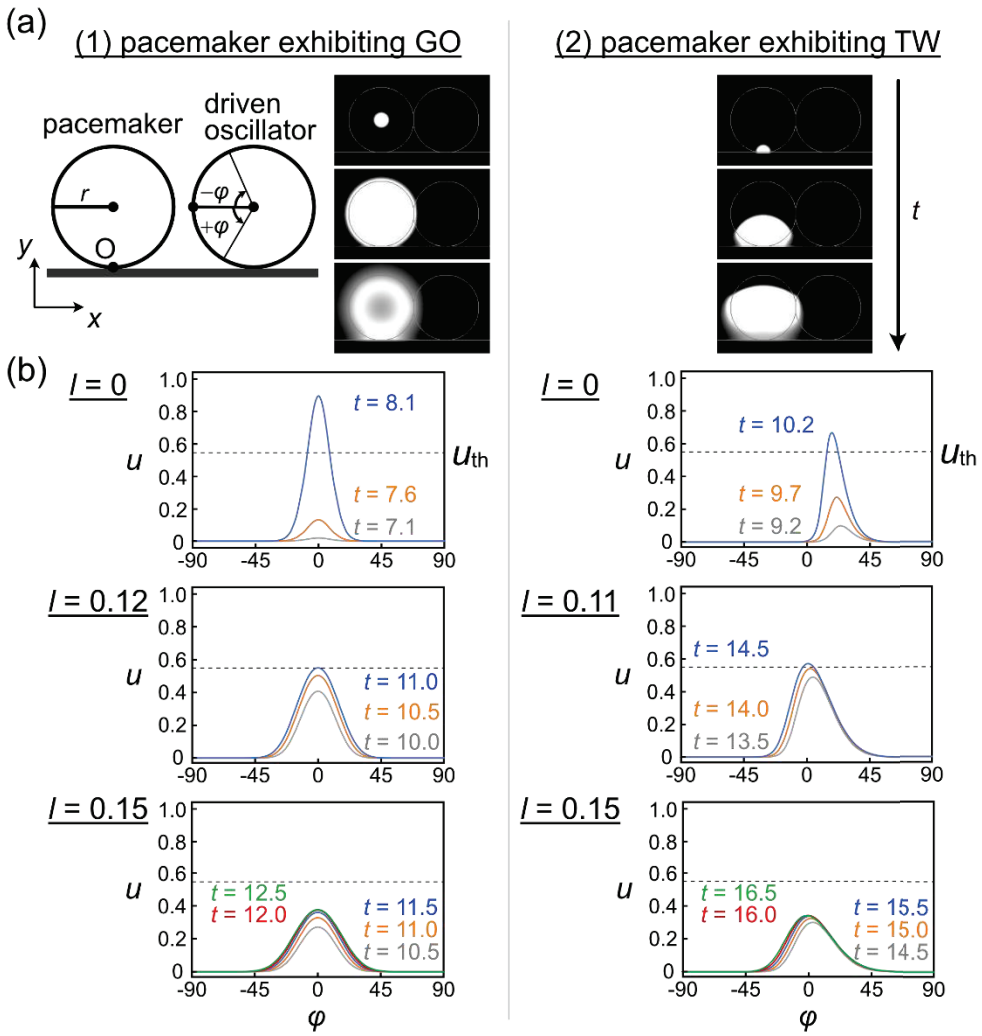

Figure 3-8. Numerical results when (1) GO and (2) TW were observed in the pacemaker (the left bead). (a) Snapshots of the two beads (time interval: (1) 7 and (2) 6). Radii of both beads, r, were set to 0.5. (b) Profiles of u depending on φ for each time t. φ was defined in (a). The profiles are plotted for three different values of l.
Reproduced from *Phys. Chem. Chem. Phys.* **2021**, *23*, 24175−24179. with permission from the PCCP Owner Societies.

In addition, the effective diffusion distance from the circumference of the

pacemaker was considered to obtain geometrically the point on the circumference of the driven oscillator, where the TW were initiated firstly. Here, this is referred to as the diffusion circle and represents the gray circle in Figure 3-9a. I assumed that the diffusion of the activator within the diffusion circle could induce the initiation of the TW in the driven oscillator. The relationship between φ and l was calculated when the diffusion circle was in contact with the right bead, as shown in Figure 3-9a. l described as:

$$l = (r_0 + r)\cos\varphi - 2r + r\sqrt{1 - \left(\frac{(r_0 + r)\sin\varphi}{r}\right)^2}, \qquad (3\text{-}4)$$

where r and r_0 are the radius of the beads and the effective diffusion distance, respectively. The values of r and r_0 were set to 0.5 and 0.11, respectively, based on the experimental results. Figure 3-9b shows the numerical results and theoretical estimation of the relationship between φ and l. φ increased with a decrease in l at $l \leq 0.11$, and this result was similar to the experimental results. These results suggest that the diffusion of the activator, $HBrO_2$, is the key factor in the synchronization in the coupled BZ bead system.

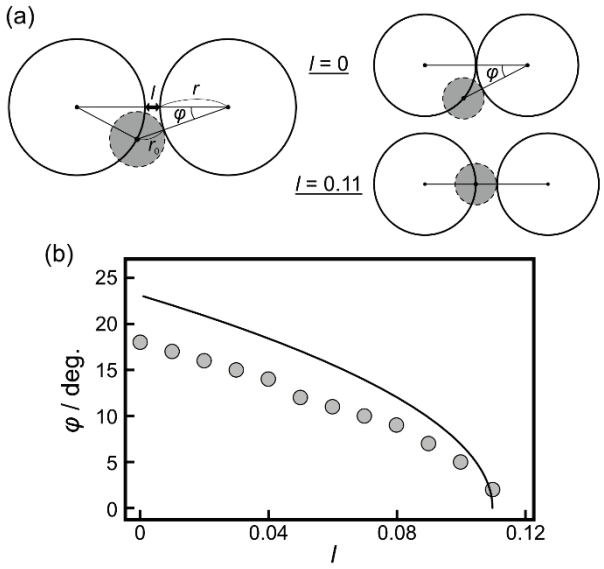

Figure 3-9. Estimation of the wave propagation in relation to the geometrical discussion. (a) Schematic illustrations and the definition of some parameters in the coupling of the two beads. (b) The results of theoretical estimation and numerical calculations for the initiation point of the TW, φ, as a function of l. The solid line and the data were obtained by eq. 3-4 and the numerical calculation in Figure 3-8, respectively.
Reproduced from *Phys. Chem. Chem. Phys.* **2021**, *23*, 24175−24179. with permission from the PCCP Owner Societies.

3-5. Conclusions

I reported that the glass and the silicone rubber plates affected the spatio-temporal patterns in the BZ bead, and they could selectively induce either the TW or the GO, respectively. In addition, several synchronized patterns were observed when the two BZ beads exhibiting TW or GO were coupled depending on the distance between the two beads. Such characteristic features of synchronization could be explained by the manner of the diffusion of the activator in the BZ reaction. I also performed the numerical calculations on the basis of the diffusion of the activator. These results have a good agreement with the experimental results, but the results indicate that we should consider the velocity of the propagating chemical waves in the pacemaker since it affects the directions of the TW. These facts suggest that the diffusion of the activator governs the synchronization of the beads, and the coupling in the BZ bead system can be regarded as the excitatory coupling rather than the inhibitory coupling.

Chapter 4: Control of Spatio-Temporal Oscillations on Microbeads in the Belousov-Zhabotinsky Reaction by Electrical Potential

4-1. Introduction

Spatio-temporal development in the BZ system can be controlled externally by the application of perturbation, for example, light irradiation[52-54] and external electric fields.[55-57] These systems continue to provide interesting insights into the mechanisms of dissipative pattern formation, and suggest that their spatio-temporal dynamics can be controlled effectively. For instance, the features of chemical wave propagation could be controlled by the application of electric field in previous studies.[55-57]

As for the pattern formation in the BZ bead system, Aihara et al. reported two distinct types of spatio-temporal patterns, i.e., global oscillations (GO) and traveling waves (TW).[33] The existence of them depends on the diameter of the bead, but surprisingly, they also observed the coexistence of GO and TW at an intermediate size range. To clarify the mechanism of switching between the two oscillatory states and their bistability, I examined the electrical control of pattern formation in the BZ beads by application of electrical potential. In addition, the mode change between two states as a function of the applied electrical potential was investigated. I also focused on the effect of sizes of the BZ beads and scanning directions of the electrical potential on the switching of patterns. The mode selection of GO and TW was discussed in relation to electrochemical reactions and the concentrations of the BZ reaction's activator, $HBrO_2$, and its inhibitor, Br^- around the BZ bead.

4-2. Experiments

The used reagents and the concentrations in the catalyst-free BZ solution were the same as the experiments in the chapter 2. The preparation of the BZ bead was also the same as reported in the previous chapters, but only the 3D-loaded beads were used in this experiment. The observation of the bead was started 2 hours after I immersed the BZ bead into the catalyst-free BZ solution (t = 120 min) to obtain stable oscillations. All experiments were carried out at 298 ± 1 K.

Figure 4-1 shows a schematic of the experimental setup for the electrical controlled the BZ bead system. A rectangular vessel (length: 70 mm, width: 45 mm) filled with the BZ solution without catalyst (depth of BZ solution: 5 mm) was used to monitor with a digital video camera from the side. The two-electrode setup consists of a platinum plate (45 mm × 5 mm, thickness: 0.1 mm) used as the working electrode and a platinum disk electrode (diameter: 1 mm) was used as the counter electrode with the reference electrode. A single 3D-loaded bead was placed on a Pt plate electrode. Application of the voltage was performed using a potentiostat (NIKKO KEISOKU, NPGS-2501-10nA, Japan) via the function generator (YOKOGAWA, FG120, Japan). The platinum disk electrode was set 2 mm away from the platinum plate. The oscillations and wave propagation in the BZ beads were analyzed using ImageJ software based on the procedures described in the chapter 2.

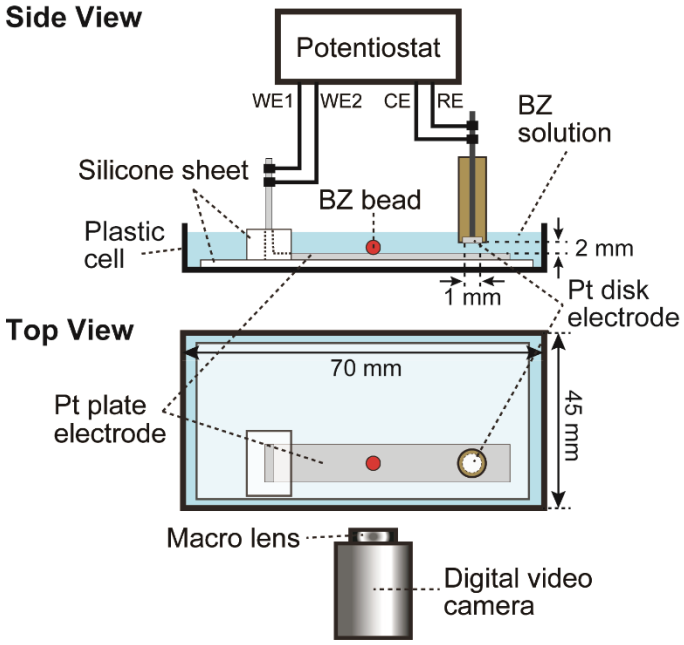

Figure 4-1. Schematics of the experimental setup to apply an electrical potential to the BZ bead. WE, CE, and RE refer to the working, counter, and reference electrodes, respectively. A single BZ bead was placed on a Pt plate electrode.
Reprinted with permission from *J. Phys. Chem. A* **2019**, *123*, 4853−4857. Copyright 2019 American Chemical Society.

In this study, I applied the electrical potential, E, to the BZ bead in two different ways; 1) the constant value of E was applied., 2) the scanning of E was carried out. To avoid the generation of O_2 bubbles on the electrode at $E > 1$ V, E was applied between −1 and +1 V. In the scanning of E, E was changed linearly at 0.8 mV s^{-1} from +1 to −1 V (negative scan), and then turned from −1 to +1 V (positive scan). I examined the different scanning profiles, for example, scanning from −1 V to +1 V, and then turned from +1 V to −1 V, but similar results were obtained. The range of the bead diameter was around 0.6 mm and 0.40−1.10 mm in experiments 1 and 2, respectively.

4-3. Results

4-3-1. The spatio-temporal oscillations under application of the constant value of the electrical potential

In this section, the effect of E on the oscillations in the BZ bead was investigated. In order to induce either GO or TW, the bead whose diameter, d, was around 0.6 mm was selected. Figure 4-2 shows the probability of the occurrence of TW or GO in the BZ beads as a function of E. A total of 100 experiments (ten for each E value) was examined to obtain these results. Here, the constant value of E was applied during t = 120−240 min, where t = 0 min corresponds to the time when the bead is firstly soaked into the BZ solution. Only TW appeared at $E \leq -0.75$ V, and the TW were initiated from the contact point between the plate electrode and the bead. On the other hand, only GO were observed at 0.50 V $\leq E \leq$ 0.75 V. Here, the oxidation was initiated from the inside of the bead. At the intermediate range of E, that is, −0.50 V $\leq E \leq$ 0.25 V, either TW or GO were observed. The pattern which was observed at t = 120 min was maintained for 2 hours. The BZ bead did not change from the reduced state at $E \geq$ 1.00 V, and thus, no oscillations were observed.

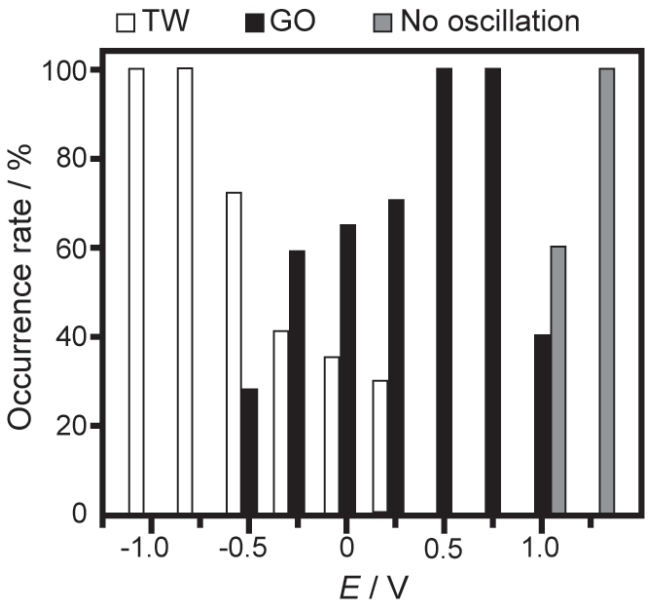

Figure 4-2. Occurrence rate of different states in the BZ beads as a function of an electrical potential, *E*. The diameter of the bead was $d \sim 0.6$ mm. Black, white, and gray bars correspond to GO, TW, and no oscillations, respectively.
Reprinted with permission from *J. Phys. Chem. A* **2019**, *123*, 4853−4857. Copyright 2019 American Chemical Society.

Figure 4-3 shows the periods of oscillations as a function of *E*. According to the results, the periods of GO did not depend on *E*, but the periods of TW increased with an increase in *E*. TW and GO coexisted at $-0.50\ \text{V} \leq E \leq 0.25\ \text{V}$, and the periods of TW were shorter than those of GO.

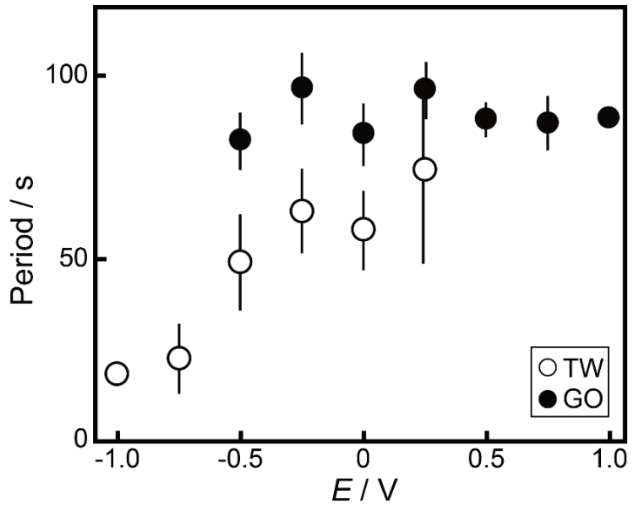

Figure 4-3. Oscillation periods as a function of *E*. The data correspond to those in Figure 4-2.
Reprinted with permission from *J. Phys. Chem. A* **2019**, *123*, 4853−4857. Copyright 2019 American Chemical Society.

In order to observe the reversible switching between GO and TW in the same BZ bead, *E* was changed periodically. In this experiment, *E* was changed at *t* = 140 min, and the initial value of *E* was zero (*t* = 120-140 min). If GO appeared at *E* = 0 V, I changed *E* to −0.75 V at *t* = 140 min to observe TW. By contrast, I changed *E* to +0.75 V at *t* = 140 min to observe GO if TW appeared at *E* = 0 V. And then, *E* was changed periodically between +0.75 V and −0.75 every 20 min, as shown in Figures 4-4a-1 and 4-4b-1.

Figures 4-4a-2 and 4-4b-2 show the time series of the oscillation periods when (a) GO or (b) TW appeared at *E* = 0 V. GO and TW appeared alternately, and their appearance was observed at the positive and negative values of *E*, respectively. Thus, GO and TW could be reversibly induced by the application of the positive and negative potential regardless of whether the initial condition, and I could reversibly select these patterns by the electrical potential.

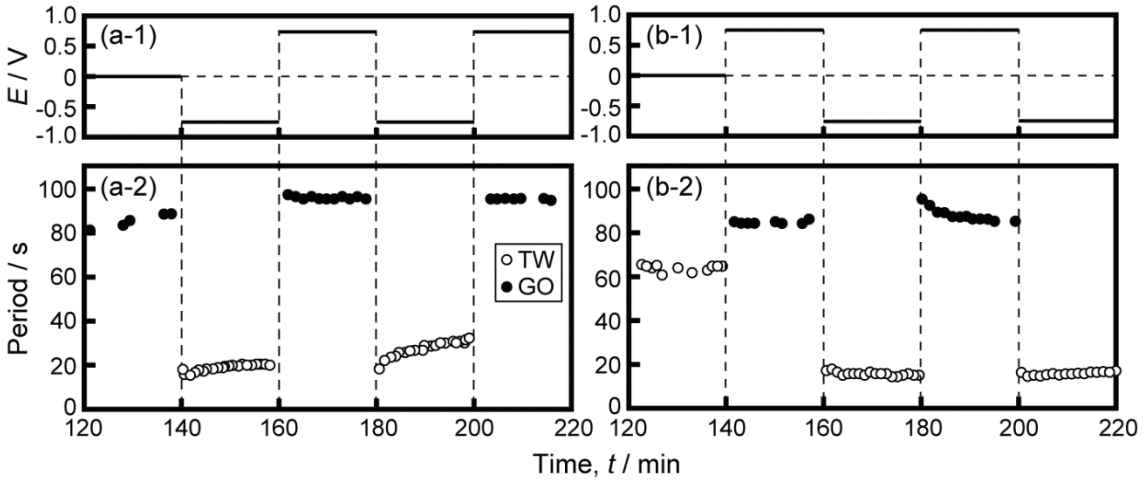

Figure 4-4. Time series of (1) E and (2) oscillation periods when (a) GO or (b) TW was observed at E = 0 V at t = 120 min. Filled and empty circles represent GO and TW, respectively.
Reprinted with permission from *J. Phys. Chem. A* **2019**, *123*, 4853−4857. Copyright 2019 American Chemical Society.

4-3-2. The spatio-temporal oscillations under application of the scanning electrical potential

Oscillatory behavior under the scanning of E depending on the size of the bead was investigated. According to the results in Figure 2-5b, the spatio-temporal patterns in the 3D-loaded beads were classified into three types depending on the diameter of the bead, d. We could observe only GO, either GO or TW, and only TW in small, middle, and large beads, respectively. Figure 4-5 shows the initiation point of the oscillations, $R_l = l_a/d$, for three different d as a function of E, where l_a corresponds to the length between the contact point with the Pt plate electrode and the initiation point of the oscillations. I distinguished whether TW or GO appeared based on the value of R_l; TW appeared if R_l was lower than 0.2, and GO appeared if $0.2 < R_l \leq 0.6$. However, $R_l > 0.6$ was not observed in the present experiment. E = −0.75 and +0.5 V were sufficient to induce TW and GO, respectively, in any size of the beads. The switching from GO to TW and from TW to GO

occurred at E_{GT} and E_{TG}, respectively, where E_{GT} and E_{TG} correspond to the electrical switching potential from GO to TW and from TW to GO, respectively. The value of E_{GT} increased with an increase in d. Especially, for the middle bead, hysteresis between E_{GT} and E_{TG} was observed clearly, as shown in Figure 4-5b. No oscillations were observed at $+0.5 < E < +1$ V in the negative scan of E when the bead size was small, as shown in Figure 4-5a.

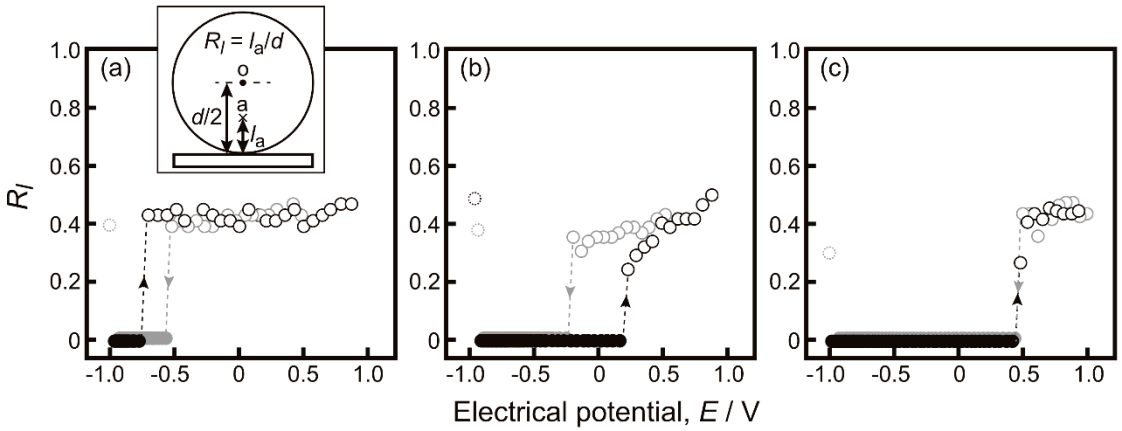

Figure 4-5. The initiation point of the oscillations, R_l, at the scanning of the electrical potential, E (Diameters of the beads, d: (a) 0.52, (b) 0.63, and (c) 1.02 mm). Filled and empty circles correspond to TW and GO, respectively. Gray and black circles represent the negative and positive scans, respectively. The definition of R_l is shown in (a) schematically. d, a, o, and l_a in (a) correspond to the diameter of the bead, the initiation point of the oscillations, the center of the bead, and the length between the contact point with the plate electrode and the point of a.

Next, the switching potential between TW and GO, E_{GT} or E_{TG}, depending on the size of the bead and the scanning direction of E was investigated. Figure 4-6 represents the switching diagram between TW and GO depending on E_{GT} or E_{TG} and d. In the negative scan, i.e., $dE/dt < 0$, E_{GT} increased with an increase in d. For smaller beads ($0.4 < d < 0.6$ mm), E_{TG} in the positive scan, i.e., $dE/dt > 0$, were similar to E_{GT} during the

scan with dE/dt < 0 (see Figures 4-5a and 4-6). In other words, I observed no hysteresis or slight hysteresis that E_{TG} was lower than E_{GT} (see Figure 4-6a) in the case of using small beads. By contrast, for middle beads (0.6 < d < 0.8 mm), E_{TG} at the scan with dE/dt > 0 were apparently different from those at the scan with dE/dt < 0, as indicated by the horizontal dotted lines in Figure 4-6, that is, hysteresis was observed depending on the scanning directions. In addition, the magnitude of hysteresis decreased with an increase in d.

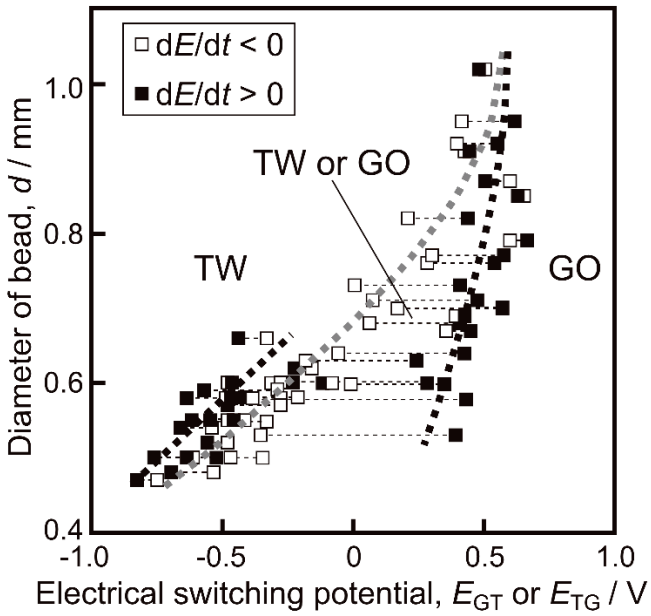

Figure 4-6. Electrical switching potential from GO to TW, E_{GT}, at the scan with dE/dt < 0 (empty rectangles) and that from TW to GO, E_{TG}, at the scan with dE/dt > 0 (filled rectangles) depending on the diameter of the BZ beads, d. The horizontal dotted lines correspond to the pair of each experiment at the positive and negative scans.

4-4. Discussion

In this section, I would like to discuss the mechanism of the spatio-temporal pattern formation under the application of the electrical potential, *E*. At first, the effect of *E* on the selection between GO and TW is discussed based on related papers.[58] Either TW and GO were observed in the middle size of the 3D-loaded bead without the effect of *E*, as shown in Figure 2-5b. These results were similar to the results reported by Aihara et al.[33] The bistability between GO and TW also existed at $-0.50\ \mathrm{V} \leq E \leq 0.25\ \mathrm{V}$ in the middle size of the bead ($d \sim 0.6$ mm). By contrast, GO and TW were selectively induced by the application of the sufficiently positive and negative potential, as shown in Figures 4-2.

In the present condition, the electrochemical reaction in eq. 4-1 on the Pt plate electrode occurred when the negative potential was applied to the BZ bead according to the previous paper.[58]

$$3H^+ + BrO_3^- + 2e^- \rightarrow HBrO_2 + H_2O \qquad (4\text{-}1)$$

The high concentration of $HBrO_2$ around the platinum plate electrode induced the bead to initiate the TW at the contact point between the plate electrode and the BZ bead.

By contrast, GO appeared under the positive potential. In this case, the oxidation of the ferroin was initiated from the bead center. This result suggests that the concentration of the inhibitor, Br^-, at the surface of the bead may be higher than that inside of the bead. The results in Fig. 4-3 which periods of GO are independent of *E* also suggest that the positive electrical potential induces neither the reaction in eq. 4-1 nor any other electrochemical reactions, and thus, the positive potential cannot break the symmetry of the distribution of the chemical species around the beads.

Next, the mechanism of the switching between TW and GO depending on *d*

under the scanning of E is discussed based on the related papers.[19,58-63]

The locations where the oscillations start are considered to discuss whether GO or TW occur. GO can be observed if the oscillations are initiated from the center of the bead, and TW appear if the oscillations start from the edge of the bead. That is, the appearance of either GO or TW is determined by the competition between the initiation of oscillations from the center of the bead or from the edge of the bead. In the BZ reaction, the autocatalytic reaction of the activator, $HBrO_2$, and the subsequent oxidation of ferroin as the autocatalytic process induce the oscillation nucleation. Thus, I should consider the periods of one BZ cycle at the center and the edge of the bead. In addition, the reaction rate from the reduced to the oxidized states at the center and the edge of the bead should be compared.

First, I consider the concentration of the activator, $[HBrO_2]$, and the inhibitor, $[Br^-]$. $[Br^-]$ should be lower than a threshold value, $[Br^-]_{crit}$, to start the autocatalytic process.[28] $[HBrO_2]$ reaches the maximum value, $[HBrO_2]_{max}$, at the end of its autocatalytic production, and subsequently $[Br^-]$ reaches the maximum value, $[Br^-]_{max}$, after the reduction of the catalyst, as a result, $[HBrO_2]$ and $[Br^-]$ oscillate during one cycle. To compare the period of one BZ cycle at the center and the edge of the bead, I need to consider two factors: 1) The time to change from $[Br^-]_{max}$ to $[Br^-]_{crit}$ becomes longer if $[Br^-]_{crit}$ is shifted to a lower value, and thus, the period becomes longer (see Figure 4-7a). 2) The time to change from $[Br^-]_{max}$ to $[Br^-]_{crit}$ becomes longer if the rate of decrease in $[Br^-]$ is slow, and as a result, the period becomes longer (see Figure 4-7b).

Second, I discuss the effect of diffusion. $HBrO_2$ produced inside the bead diffuses into the outer solution, as a result, $[HBrO_2]$ inside the bead decreases. Here, $[HBrO_2]$ at the edge of the bead rapidly decreases rather than that at the center since the

surface of the bead contacts with the external solution. I call this the boundary effect. Here, I can estimate that the rate of decrease in [$HBrO_2$] is one of the parameters to determine $[Br^-]_{crit}$ since $HBrO_2$ reacts with Br^- and consume each other in the BZ reaction. Therefore, the value of $[Br^-]_{crit}$ at the edge of the bead changes lower and the time to change from $[Br^-]_{max}$ to $[Br^-]_{crit}$ at the edge of the bead becomes longer although the rate of decrease in [Br^-] at the edge of the bead is the same as that at the center of the bead, as shown in Figure 4-7a. By contrast, the rate of decrease in [$HBrO_2$] becomes slower since the plate acts as a no-flux boundary when the BZ bead is placed and oscillates on the Pt plate. I call this the reflection effect. Due to this, $[Br^-]_{crit}$ at the edge of the bead near the electrode changes higher, and thus, the time to change from $[Br^-]_{max}$ to $[Br^-]_{crit}$ becomes shorter, as shown in Figure 4-7a. Thus, the period at the edge of the bead is shorter than that at the center of the bead when the BZ bead exhibits oscillations on the plate electrode, and we can observe TW easily. This reflection effect depends on the curvature of the bead, for example, the reflection of $HBrO_2$ easily affects the bead with the smaller curvature. Therefore, we may observe TW easily in the larger bead.

Figure 4-7b can explain the mechanism of appearance of GO or TW depending on *E* in relation to the rate of decrease in [Br^-]. Positive and negative charged particles can move around the electrode according to the Gouy-Chapman theory.[59] Application of an electrical potential allows to form the diffuse layer, whose thickness is the several to several tens nm, near the electrode. Thus, [Br^-] may become locally high around the electrode when the positive potential is applied. Therefore, the rate of decrease in [Br^-] at the edge of the bead around the electrode becomes slower than that at the center of the bead, and the time to change from $[Br^-]_{max}$ to $[Br^-]_{crit}$ also becomes longer, as shown as Figure 4-7b. Thus, the timing to switch to the autocatalytic process becomes earlier at the

center of the bead, and this induces the appearance of GO. On the other hand, $HBrO_2$ is produced by the electrochemical reaction at the negative potential, as a result, $[HBrO_2]$ around the electrode is locally high. Thus, the rate of decrease in $[Br^-]$ at the edge of the bead near the electrode is rapid, and TW appear easily.

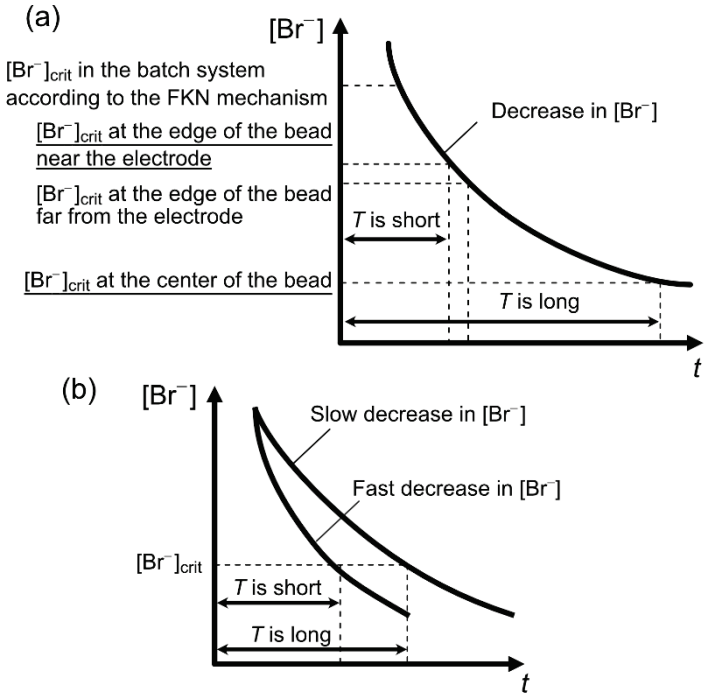

Figure 4-7. (a) Schematics for the mechanism of determination of the oscillation period, T, depending on $[Br^-]_{crit}$. (b) Schematics for the mechanism of determination of T depending on the rate of decrease in $[Br^-]$.
Reprinted with permission from *J. Phys. Chem. B* **2021**, *125*, 3638−3643. Copyright 2021 American Chemical Society.

Finally, I discuss the electrical switching potential E_{GT} or E_{TG} depending on the scanning direction of E. Here, I note that it is unclear why the distribution of E_{TG} in the positive scan is slightly lower than that of E_{GT} in the negative scan, as shown in Figure 4-6. Therefore, I discuss only large hysteresis in the middle size of the bead. The values of

E_{TG} in the positive scan were higher than that of E_{GT} in the negative scan, especially for the middle size of the bead ($d \sim 0.7$ mm). This hysteresis may be induced by the initial [Br^-] and [$HBrO_2$] which depend on the initial value of E. In the negative scan, Br^- is attracted to the electrode due to the initial positive potential, and thus, the local initial [Br^-] around the Pt plate electrode is higher than any other edge of the bead. Therefore, the transition from GO to TW is delayed, as a result, E_{GT} becomes lower. By contrast, the local initial [$HBrO_2$] around the Pt plate electrode is high in the positive scan since the initial negative potential induces the production of $HBrO_2$. Here, I note that the electrochemical reduction of bromate is an inert process, but bromate can be reduced to $HBrO_2$ electrochemically.[58,60,61] Therefore, the transition from TW to GO delays, and thus, E_{TG} becomes higher. The present work suggests spatio-temporal patterns are also deformed by the electrochemical reaction,[62,63] although the spatio-temporal patterns in the BZ bead, e.g., TW or GO, are mainly determined by those of chemicals, e.g., $HBrO_2$ or Br^-, which are the activator and inhibitor in the BZ reaction according to the FKN mechanism.[58]

4-5. Conclusions

In this chapter, spatio-temporal patterns in the ferroin-loaded bead were controlled by the application of the electrical potential, E. Two dynamic bistable states, i.e., traveling waves (TW) and global oscillations (GO), were observed at $E = 0$, but TW and GO could be selectively induced by the negative and positive potential, respectively. In addition, the reversible changes between TW and GO were observed by the periodical changes in E between sufficiently positive and negative potential.

Furthermore, I investigated the switching between TW and GO depending on E and the diameter of the beads, d, by the scanning of E. The switching from TW to GO in the positive scan occurred at the higher value of E in comparison to that from GO to TW in the negative scan, that is, hysteresis was observed.

These results were discussed in relation to the triggering oscillations based on the distribution of the activator, $HBrO_2$, or its key inhibitor, Br^-, which are produced in the electrochemical reactions. The negative potential accelerated the accumulation of $HBrO_2$ near the electrode by the electrochemical reaction, and this induced the generation of the TW at the contact point between the Pt plate electrode and the BZ bead. By contrast, the application of the positive potential could not break the symmetrical distributions of activator or inhibitor around the bead, or rather, that inhibited the generation of the TW according to the experimental results. Specifically, the distribution of Br^- around the BZ bead may play an important role in the generation of hysteresis. However, I should note that the electrical switching potentials, E_{GT} and E_{TG}, at negative potential are independent of the scanning direction of E when small beads were used, and this is still an open problem.

Chapter 5: General Conclusion

I investigated the self-organized pattern formation using the Belousov-Zhabotinsky reaction, which exhibited the chemical oscillations spontaneously. The three types of spatio-temporal patterns appeared on the surface or in the body of the spherical cation-exchange resin bead loaded with the catalyst for the BZ reaction, ferroin, i.e., global oscillations (GO), traveling waves (TW), and spiral/scroll waves (SW). I also observed the switching of the patterns by coupling the two BZ beads or application of the electrical potential to the BZ bead.

The first study (chapter 2) describes the improved experimental protocol with the BZ reaction. I prepared the "BZ bead" by loading with the catalyst for the BZ reaction either onto the surface or into the body of the cation-exchange resin beads selectively, as a result, several self-organized patterns can be observed. In addition, I found that the dynamics of spatio-temporal patterns, i.e., spatially uniform oscillations, traveling reaction fronts, and rotating spiral waves, at the vicinity of the bead are apparently different from those in the body of the bead. This experimental system enables us to observe the oscillating patterns on the heterogeneous concentration field. I believe that those results will contribute to revealing the mechanisms of wave localization in biological cells that can be constrained to the surface or the vicinity of the cell membrane.

The second study, as shown in chapter 3, clarified the changes in the propagating directions of the chemical waves affected by the external conditions. This study also investigated the network behaviors of the coupled two BZ beads. Homogeneous oscillations, GO, changed to inhomogeneous oscillations, TW, when the other bead was placed near the bead since the reaction dynamics changed drastically. This was induced

by breaking the symmetrical distributions of chemicals, such as the activator and inhibitor of the BZ reaction, around the spherical bead. In the coupling of the two beads which exhibited TW, I observed the change in the propagation direction of the TW. I discussed that based on the diffusion dynamics of the activator, and carried out the numerical calculations. These results suggest that the diffusion of the activator plays an important role in the interaction between the BZ beads and regulates the generation of the chemical waves. I believe that this study can contribute to the understanding of network behavior, for example, information transduction over the biological cells.

Chapter 4 shows the electrochemical control of the spatio-temporal oscillations in the BZ bead. Application of the constant values of the sufficient positive and negative potential to the ferroin-loaded bead in the catalyst-free BZ solution induced GO and TW, respectively. In addition, the scanning of the electrical potential, i.e., from +1 to −1 V (negative scan) and from −1 to +1 V (positive scan), triggered off the switching between GO and TW. The electrical switching potential from TW to GO, E_{TG}, in the positive scan was different from that from GO to TW, E_{GT}, in the negative scan, that is, hysteresis was observed. I also revealed that E_{TG} and E_{GT} depended on the diameter of the bead. In this chapter, these results were discussed in relation to the distribution of the chemicals produced by the electrode reaction. This study suggests that the control of oscillations in chemical systems helps to understand not only the temporal but also the spatial development of oscillatory phenomena in living organisms.

Overall, these results in this thesis can contribute to our understanding of the mechanisms of the spatio-temporal pattern formation in the spherical field. Specifically, the observation of wave phenomena in the vicinity of the surface or in the entire volume of the spherical bead is useful for the understanding of the features of synchronization

between the oscillators mediated by wave propagation. I believe that chemical experimental systems using the BZ reaction, which are combined with the numerical approach, are the key step to clarify and control the nonlinear phenomena in living organisms. For example, the oscillatory behavior and synchronized pattern formation of the BZ beads are surprisingly similar to the heartbeat phenomenon which is created by coupled myocardial cells. We use medical devices, e.g., automated external defibrillator (AED), to eliminate the fibrillation and to control the re-establishment of the beating rhythm. However, this electric shock to the whole of the cardiac body is too severe for the myocardial cells. Thus, the control of the spatio-temporal oscillations by local stimulation which is shown in chapter 4 is useful for solving those problems. Therefore, I believe that this study has a high potential to develop into engineering applications.

References

1. Allard, J.; Mogilner, A. Traveling Waves in Actin Dynamics and Cell Motility. *Curr. Opin. Cell Biol.* **2013**, *25*, 107−115.
2. Goldbeter, A. Oscillations and Waves of Cyclic AMP in Dicyostelium: A Prototype for Spatio-Temporal Organization and Pulsatile Intercellular Communication. *Bull. Math. Biol.* **2006**, *68*, 1095−1109.
3. Winfree, A. T. *The Geometry of Biological Time*; Springer: New York, 1980.
4. Denda, M.; Denda, S. Air-exposed Keratinocytes Exhibited Intracellular Calcium Oscillation. *Skin Res. Technol.* **2007**, *13*, 195− 201.
5. Kondo, S.; Miura, T. Reaction-Diffusion Model as a Framework for Understanding Biological Pattern Formation. *Science* **2010**, *329*, 1616−1620.
6. Lechleiter, J.; Girard, S.; Peralta, E.; Clapham, D. Spiral Calcium Wave Propagation and Annihilation in Xenopus Laevis Oocytes. *Science* **1991**, *252*, 123−126.
7. Bessho, Y.; Kageyama, R. Oscillations, Clocks and Segmentation, *Curr. Opin. Genet. Dev.* **2003**, *13*, 379−384.
8. Masamizu, Y.; Ohtsuka, T.; Takashima, Y.; Nagahara, H.; Takenaka, Y.; Yoshikawa, K.; Okamura, H.; Kageyama, R. Real-time Imaging of the Somite Segmentation Clock: Revelation of Unstable Oscillators in the Individual Presomitic Mesoderm Cells. *Proc. Natl. Acad. Sci. U.S.A.* **2006**, *103*, 1313–1318.
9. Yoshioka-Kobayashi, K.; Matsumiya, M.; Niino, Y.; Isomura, A.; Kori, H.; Miyawaki, A.; Kageyama, R. Coupling Delay Controls Synchronized Oscillation in the Segmentation Clock. *Nature* **2020**, *580*, 119–123.
10. Kuramoto, Y. *Chemical Oscillations, Waves, and Turbulence*, Springer, New York,

1984.

11. Pikovsky, A.; Rosenblum, M.; Kurths, J. Synchronization, *A Universal Concept in Nonlinear Sciences*, Cambridge University Press, Cambridge, 2001, 266–278.
12. Luther, S.; Fenton, F. H.; Kornreich, B. G.; Squires, A.; Bittihn, P.; Hornung, D.; Zabel, M.; Flanders, J.; Gladuli, A.; Campoy, L. *et al*., Low-energy Control of Electrical Turbulence in the Heart. *Nature* **2011**, *475*, 235–239.
13. Davidenko, J. M.; Pertsov, A. V.; Salomonsz, R.; Baxter, W.; Jalife, J. Stationary and Drifting Spiral Waves of Excitation in Isolated Cardiac Muscle. *Nature* **1992**, *355*, 349–351.
14. Gray, R. A.; Pertsov, A. M.; Jalife, J. Spatial and Temporal Organization During Cardiac Fibrillation. *Nature* **1998**, *392*, 75–78.
15. Witkowski, F. X.; Leon, L. J.; Penkoske, Wayne P. A.; Giles, R.; Spano, M. L.; Ditto, W. L. Winfree A. T. Spatiotemporal Evolution of Ventricular Fibrillation. *Nature* **1998**, *392*, 78–82.
16. Cherry, E. M.; Fenton, F. H. Visualization of Spiral and Scroll Waves in Simulated and Experimental Cardiac Tissue. *New J. Phys.* **2008**, *10*, 125016–125059.
17. Zaikin, A. N.; Zhabotinsky, A. M. Concentration Wave Propagation in Two-Dimensional Liquid-Phase Self-Oscillating System. *Nature* **1970**, *225*, 535−537.
18. Kapral, R., Showalter, K., *Eds. Chemical Waves and Patterns*; Kluwer Academic: Dordrecht, The Netherlands, 1995.
19. Field, R. J.; Burger, M. *Oscillations and Traveling Waves in Chemical Systems, 1st ed.*; Wiley: New York, 1985.
20. Winfree, A. T. Spiral Waves of Chemical Activity. *Science* **1972**, *175*, 634−636.
21. Winfree, A. T. Scroll-Shaped Waves of Chemical Activity in Three Dimensions.

Science **1973**, *181*, 937−939.

22. Steinbock, O.; Müller, S. C. Radius-Dependent Inhibition and Activation of Chemical Oscillations in Smaller Droplets. *J. Phys. Chem. A* **1998**, *102*, 6485−6490.
23. Kitahata, H.; Aihara, R.; Magome, N.; Yoshikawa, K. Convective and Periodic Motion Driven by a Chemical Wave. *J. Chem. Phys.* **2002**, *116*, 5666−5672.
24. Kitahata, H.; Yoshinaga, N.; Nagai, K.; Sumino, Y. Spontaneous Motion of a Belousov-Zhabotinsky Reaction Droplet Coupled with a Spiral Wave. *Chem. Lett.* **2012**, *41*, 1052−1054.
25. Yamaguchi, T.; Kuhnert, L.; Nagy-Ungvarai, Z.; Mueller, S. C.; Hess, B. Gel Systems for the Belousov-Zhabotinskii Reaction. *J. Phys. Chem.* **1991**, *95*, 5831−5837.
26. Guo, D.; Li, Y.; Zheng, B. A Microreactor and Imaging Platform for Studying Chemical Oscillators. *J. Phys. Chem. A* **2013**, *117*, 6402− 6408.
27. Thutupalli, S.; Seemann, R.; Herminghaus, S. Swarming Behavior of Simple Model Squirmers. *New J. Phys.* **2011**, *13*, 073021.
28. Suematsu, N. J.; Mori, Y.; Amemiya, T.; Nakata, S. Oscillation of Speed of a Self-Propelled Belousov-Zhabotinsky Droplet. *J. Phys. Chem. Lett.* **2016**, *7*, 3424−3428.
29. Suematsu, N. J.; Saikusa, K.; Nagata, T.; Izumi S. Interfacial Dynamics in the Spontaneous Motion of an Aqueous Droplet. *Langmuir* **2019**, *35*, 11601–11607.
30. Suematsu, N. J.; Mori, Y.; Amemiya, T.; Nakata, S. Spontaneous Mode Switching of Self-Propelled Droplet Motion Induced by a Clock Reaction in the Belousov−Zhabotinsky Medium. *J. Phys. Chem. Lett.* **2021**, *12*, 7526−7530.
31. Maselko, J.; Showalter, K. Chemical Waves on Spherical Surfaces. *Nature* **1989**, *339*, 609−611.
32. Yoshikawa, K.; Aihara, R.; Agladze, K. Size-Dependent Belousov-Zhabotinsky

Oscillation in Small Beads. *J. Phys. Chem. A* **1998**, *102*, 7649−7652.

33. Aihara, R.; Yoshikawa, K. Size-Dependent Switching of the Spatiotemporal Structure between a Traveling Wave and Global Rhythm. *J. Phys. Chem. A* **2001**, *105*, 8445−8448.
34. Suzuki, K.; Yoshinobu, T.; Iwasaki, H. Diffusive Propagation of Chemical Waves through a Microgap. *J. Phys. Chem. A* **2000**, *104*, 5154-5159.
35. Zykov, V. S.; Müller, S. C. Controlling Spiral Waves in Confined Geometries by Global Feedback. *Phys. Rev. Lett.* **1997**, *78*, 3398-3401.
36. Gomatam, J.; Amdjadi, F. Reaction-Diffusion Equations on a Sphere: Meandering of Spiral Waves. *Phys. Rev. E* **1997**, 56, 3913-3919.
37. Nishiyama, N.; Eto, K. Experimental Study on Three Chemical Oscillators Coupled with Time Delay. *J. Chem. Phys.* **1994**, *100*, 6977− 6978.
38. Miyakawa, K.; Okabe, T.; Mizoguchi, M.; Sakamoto, F. Synchronization in the Discrete Chemical Oscillation System. *J. Chem. Phys.* **1995**, *103*, 9621−9625.
39. Fukuda, H.; Tamari, N.; Morimura, H.; Kai, K. Entrainment in a Chemical Oscillator Chain with a Pacemaker. *J. Phys. Chem. A* **2005**, *109*, 11250−11254.
40. Toiya, M.; Gonzalez-Ochoa, H. O.; Vanag, V. K.; Fraden, S.; Epstein, I. R. Synchronization of Chemical Micro-oscillators. *J. Phys. Chem. Lett.* **2010**, *1*, 1241 −1246.
41. Mallphanov, I. L.; Vanag, V. K. Distance Dependent Types of Coupling of Chemical Micro-Oscillators Immersed in a Water-in-Oil Microemulsion. *Phys. Chem. Chem. Phys.* **2021**, *23*, 9130−9138.
42. Nkomo, S.; Tinsley, M. R.; Showalter, K. Chimera States in Populations of Nonlocally Coupled Chemical Oscillators. *Phys. Rev. Lett.* **2013**, *110*, 244102.

43. Gorecki, J., Gorecka, J. N. Adamatzky, A. Information Coding with Frequency of Oscillations in Belousov-Zhabotinsky Encapsulated Disks. *Phys. Rev. E* **2014**, *89*, 042910.

44. Chen, T.; Tinsley, M. R.; Ott, E.; Showalter, K. Echo Behavior in Large Populations of Chemical Oscillators. *Phys. Rev. X* **2016**, *6*, 041054.

45. Adamatzky, A. A Brief History of Liquid Computers. *Philos. Trans. R. Soc., B* **2019**, *374*, 20180372.

46. Vanag, V. K. Hierarchical Network of Pulse Coupled Chemical Oscillators with Adaptive Behavior: Chemical Neurocomputer. *Chaos* **2019**, *29*, 083104

47. Gaspar, V.; Bazsa, G.; Beck, M. The Influence of Visible Light on the Belousov-Zhabotinskii Oscillating Reactions Applying Different Catalysts. *Z. Phys. Chem.* **1983**, *264*, 43−48.

48. Kohl, P.; Hunter, P.; Noble, D. Stretch-Induced Changes in Heart Rate and Rhythm: Clinical Observations, Experiments and Mathematical Models. *Prog. Biophys. Mol. Biol.* **1999**, *71*, 91−138.

49. Brunello, L.; Slabaugh, J. L.; Radwański, P. B.; Ho, H. T.; Belevych, A. E.; Lou, Q.; Chen, H.; Napolitano, C.; Lodola, F.; Priori, S. G. *et al*., Decreased RyR2 Refractoriness Determines Myocardial Synchronization of Aberrant Ca^{2+} Release in a Genetic Model of Arrhythmia. *Proc. Natl. Acad. Sci. U.S.A.* **2013**, *110*, 10312.

50. Weber, A.; Prokazov, Y.; Zuschratter, W.; Hauser, M. J. B. Desynchronisation of Glycolytic Oscillations in Yeast Cell Populations. *PLoS One* **2012**, *7*, e43276.

51. Amemiya, T.; Shibata, K.; Itoh, Y.; Itoh, K.; Watanabe, M.; Yamaguchi, T.; Primordial Oscillations in Life: Direct Observation of Glycolytic Oscillations in Individual HeLa Cervical Cancer Cells. *Chaos* **2017**, *27*, 104602.

52. Kuhnert, L. A New Optical Photochemical Memory Device in a Light-Sensitive Chemical Active Medium. *Nature* **1986**, *319*, 393− 394.

53. Nishi, K.; Suzuki, S.; Kayahara, K.; Kuze, M.; Kitahata, H.; Nakata, S.; Nishiura, Y. Achilles' heel of a traveling pulse subject to a local external stimulus. *Phys. Rev. E* **2017**, *95*, 062209.

54. Gizynski, K.; Gorecki, J. Chemical Memory with States Coded in Light Controlled Oscillations of Interacting Belousov−Zhabotinsky Droplets. *Phys. Chem. Chem. Phys.* **2017**, *19*, 6519−6531.

55. Ševčíková, H.; Marek, M. Chemical Waves in Electric Field. *Phys. D* **1983**, *9*, 140−156.

56. Ševčíková, H.; Marek, M. Chemical Front Waves in an Electric Field. *Phys. D* **1984**, *13*, 379−386.

57. Ševčíková, H.; Marek, M.; Müller, S. C. The Reversal and Splitting of Waves in an Excitable Medium Caused by an Electrical Field. *Science* **1992**, *257*, 951−954.

58. Field, R. J.; Körös, E.; Noyes, R. M. Oscillations in Chemical Systems. II. Thorough Analysis of Temporal Oscillation in the Bromate-Cerium-Malonic Acid System. *J. Am. Chem. Soc.* **1972**, *94*, 8649−8664.

59. Bard, A. J.; Faulkner, L. R. *Electrochemical Methods: Fundamentals and Applications*; John Wiley & Sons, Inc.: New York, 2001.

60. Badea, G. E.; Badea, T. Kinetics and Mechanism of the Bromate Electrochemical Reduction at Platinum Electrode. *Rev. Roum. Chim*. **2006**, *51*, 127−133.

61. Kishimoto, N.; Matsuda, N. Bromate Ion Removal by Electrochemical Reduction Using an Activated Carbon Felt Electrode. *Environ. Sci. Technol.* **2009**, *43*, 2054−2059.

62. Vorotyntsev, M. A.; Antipov, A. E. Bromate Electroreduction from Acidic Solution at Rotating Disc Electrode. Theory of Steady-state Convective-diffusion Transport. *Electrochim. Acta* **2017**, *246*, 1217−1229.

63. Modestov, A. D.; Konev, D. V.; Antipov, A. E.; Petrov, M. M.; Pichugov, R. D.; Vorotyntsev, M. A. Bromate Electroreduction from Sulfuric Acid Solution at Rotating Disk Electrode: Experimental Study. *Electrochim. Acta* **2018**, *259*, 655−663.

Acknowledgements

This study has been supervised by Professor Nakata Satoshi from 2017 to 2019 at the Graduate School of Science, and from 2019 to 2022 at the Graduate School of Integrated Sciences for Life, Hiroshima University. This work would not have been possible without the constant support, guidance, and assistance of Prof. Satoshi Nakata. Also, he has always encouraged me in the present study, and provided invaluable feedback on my report, at times responding to emails late at night and early in the morning. I sincerely appreciate his great kindness.

I thank sub-supervisors, Prof. Shunsuke Izumi, Associate Prof. Yoshihisa Fujiwara, and Associate Prof. Shinpei Tanaka, for useful discussion. I would like to express my gratitude to Assistant Prof. Masao Fujiwara and Assistant Prof. Muneyuki Matsuo for their support.

I acknowledge the financial support from Japan Society for the Promotion of Science since this study was supported by JSPS Research Fellowships for Young Scientists from 2020 to 2022 (JSPS KAKENHI Grant JP20J14555).

I would like to be grateful for their guidance and encouragement to the following collaborators: Prof. Oliver Steinbock, Prof. Takashi Amemiya, Prof. Akihisa Shioi, Prof. Hiroyuki Kitahata, Associate Prof. Nobuhiko J. Suematsu, Dr. Yasunao Okamoto, Ms. Yuri Hiranishi, and Ms. Mari Horisaka.

Also, I give all of the members in Nakata's lab my gratitude.